Integrated In Silico and In Vivo Evaluation of the Antiepileptic Potential of Chenopodium album L. in a Pentylenetetrazole-Induced Seizure Model

Naznin Sarkar
Visveswarapura Institute of Pharmaceutical Sciences
Anil Kumar Venkategowda Kodihally
anilkumargcp@rediffmail.com

Visveswarapura Institute of Pharmaceutical Sciences
Bharath Kumar Chagaleti
SRM College of Pharmacy, Faculty of Medicine and Health Sciences, SRM Institute of Science and Technology

---

Research Article

Keywords: Chenopodium album L., Epilepsy, Pentylenetetrazole, Network pharmacology, Molecular docking, STAT3, Molecular dynamics simulation

Posted Date: August 14th, 2026

DOI: https://doi.org/10.21203/rs.3.rs-10301958/v1

Additional Declarations: No competing interests reported.

Integrated *In Silico* and *In Vivo* Evaluation of the Antiepileptic Potential of *Chenopodium album* L. in a Pentylenetetrazole-Induced Seizure Model

Naznin Sarkar[1], Anil Kumar Venkategowda Kodihally [*1], Bharath Kumar Chagaleti[2]

[1]Visveswarapura Institute of Pharmaceutical Sciences, Bengaluru, 560070, Karnataka, India,
[2]Department of Pharmaceutical Chemistry, SRM College of Pharmacy, Faculty of Medicine and Health Sciences, SRM Institute of Science and Technology, Kattankulathur, Chengalpattu, 603203, Chennai, India

***Corresponding author**:
Dr. Anil Kumar K V, Department of Pharmacology, Visveswarapura Institute of Pharmaceutical Sciences, Bengaluru- 560070, Karnataka, India. Email. ID: anilkumargcp@rediffmail.com

Abstract

Background: Epilepsy is a multifactorial disorder of the central nervous system characterized by recurrent, unprovoked seizures resulting from abnormal neuronal activity. Despite available antiepileptic drugs, treatment is limited by drug resistance and adverse effects, highlighting the need for safer agents. This study investigated the anticonvulsant potential of *Chenopodium album* L. using an integrated computational and experimental approach.

Methods: Methanolic leaf extract of *Chenopodium album* was analysed by LC–MS to identify phytoconstituents. Network pharmacology, Gene Ontology (GO), Kyoto Encyclopedia of Genes and Genomes (KEGG) pathway enrichment, molecular docking, molecular dynamics simulation, MM-GBSA, principal component analysis (PCA), free energy landscape (FEL), and ADMET prediction were performed. Anticonvulsant activity was validated in the pentylenetetrazole (PTZ)-induced seizure model in mice.

Results: LC–MS identified 27 phytoconstituents. Network pharmacology revealed 541 overlapping targets between *C. album* phytoconstituents and epilepsy-related genes, with STAT3 as the key hub protein. Enrichment analysis highlighted EGFR tyrosine kinase inhibitor resistance, JAK–STAT, HIF-1, and estrogen signalling pathways. Quercetin showed the highest affinity for STAT3, while molecular dynamics, MM-GBSA, PCA, and FEL analyses confirmed a stable quercetin–STAT3 complex. ADMET prediction indicated favorable pharmacokinetic properties. The *in vivo* anticonvulsant activity of the methanolic leaf extract was confirmed in the pentylenetetrazole-induced seizure model, where treatment significantly delayed seizure onset and

reduced seizure duration in a dose-dependent manner, with complete seizure protection observed at 400 mg/kg, comparable to ethosuximide.

Conclusions: *Chenopodium album* exhibited significant anticonvulsant activity by modulating multiple molecular targets, particularly STAT3, supporting its potential as multi-target therapeutic candidate for epilepsy.

Keywords: *Chenopodium album* L.; Epilepsy; Pentylenetetrazole; Network pharmacology; Molecular docking; STAT3; Molecular dynamics simulation.

1. Introduction:

Natural compounds obtained from plants have been widely explored as a valuable source for the development of new medicines. Their chemical complexity and wide range of biological activities make them suitable candidates for treating many chronic and multifactorial diseases [1,2]. In recent years, increasing attention has been given to medicinal plants in neurological research, as their bioactive constituents may influence multiple pathways involved in disorders such as epilepsy.

Chenopodium album L. belonging to the family Amaranthaceae and popularly known as bathua, is a widely distributed edible medicinal plant traditionally used across Asia, Europe, and Africa. In traditional medicine, it has been employed as a nervine tonic, anti-inflammatory agent, laxative, anthelmintic, diuretic, and analgesic, indicating relevance in central nervous system (CNS) disorders [3, 4, 5]. Phytochemical studies have revealed that *C. album* contains flavonoids, phenolic acids, terpenoids, saponins, and glycosides with antioxidant, anti-inflammatory, and neuromodulatory properties [3,6].

Experimental studies demonstrate strong antioxidant and anti-inflammatory activities of *C. album,* largely attributed to its high phenolic and flavonoid content [6,7]. Oxidative stress and neuroinflammation are key contributors to epileptogenesis, neuronal injury, and seizure propagation. Excessive reactive oxygen species and inflammatory mediators disrupt GABAergic neurotransmission, alter ion channel function, and promote neuronal hyperexcitability [8,9]. Furthermore, emerging evidence indicates that multiple intracellular signalling pathways involved in inflammation, cell survival, and neuronal plasticity contribute to seizure development and progression. Therefore, modulation of these interconnected molecular networks may represent a promising strategy for epilepsy management [10].

Beyond antioxidant effects, *C. album* exhibits antidepressant, analgesic, spasmolytic, hepatoprotective, and neuromodulatory activities in experimental models [11,12,13].These effects

are particularly relevant as mood disorders, neurotransmitter imbalance, and neuroinflammation commonly coexist with epilepsy[14,15]. Spasmolytic and ion-channel-modulating actions further suggest interactions with calcium and potassium channels involved in seizure initiation and propagation [12].

Epilepsy affects over 50 million people globally, with nearly 80% of cases occurring in low- and middle-income countries [16]. Although several antiepileptic drugs are available, long-term therapy is often associated with adverse effects, cognitive impairment, teratogenicity, hepatotoxicity, and pharmacoresistance, highlighting the need for safer multitarget alternatives [17].

The pentylenetetrazole (PTZ)-induced seizure model is widely used to evaluate myoclonic and absence-like seizures. PTZ induces seizures by antagonizing $GABA_A$ receptors, leading to reduced inhibitory neurotransmission and neuronal hyperexcitability [18]. Seizure severity is commonly assessed using the Racine scale [19, 20]. Although PTZ acts via GABAergic inhibition, absence and myoclonic seizures critically involve thalamocortical synchronization mediated by T-type Ca^{2+} channels; accordingly, ethosuximide, the standard reference drug, suppresses seizures through T-type Ca^{2+} channel inhibition [21].

Although *Chenopodium album* has been investigated for several pharmacological activities, its antiepileptic potential has not been systematically examined using an integrated computational and experimental framework. The present study therefore combined network pharmacology, molecular docking, molecular dynamics simulation, ADMET prediction, and PTZ-induced seizure evaluation to investigate the molecular mechanisms and anticonvulsant activity of *C. album*.

2. Materials and methods

2.1. Laboratory experiments

2.1.1. Plant Authentication and Extraction:

The leaves of *Chenopodium album* L. were collected in January 2025 from Dhubri, Assam, India, and authenticated by Dr. V. Rama Rao, Research Officer (Botany), Central Ayurveda Research Institute, Ministry of AYUSH, Government of India (Ref. No.: RRCBI-18022). The leaves were shade-dried, coarsely powdered, and extracted using a Soxhlet apparatus with 99.8% methanol for 10–12 cycles. The extract was concentrated at 45 °C and dried. Methanol was selected as the extraction solvent based on earlier reports demonstrating its efficiency in extracting phenolic and flavonoid constituents associated with antioxidant and neuroactive properties [3].

2.1.2. Preliminary Phytochemical Analysis of Methanolic *Chenopodium album* Leaf Extract: Preliminary phytochemical screening of the methanolic leaf extract of *Chenopodium album* was carried out using standard qualitative tests to detect the presence of alkaloids, flavonoids, phenolic compounds, tannins, saponins, glycosides, steroids, triterpenoids, carbohydrates, proteins, and amino acids.

2.1.3. Liquid Chromatography–Mass Spectrometry (LC–MS) Analysis of Methanolic Leaf Extract of *Chenopodium album* L.: The methanolic leaf extract of *Chenopodium album* was analyzed by LC–MS for qualitative phytochemical profiling using a Waters 2695 Alliance HPLC coupled with a Micromass ZQ mass spectrometer (MassLynx software). Separation was achieved on an Inertsil ODS-3 column (4.6 × 100 mm, 3 µm) using a mobile phase consisting of 0.1% formic acid in water (A) and acetonitrile (B) at a flow rate of 1.0 mL/min. A gradient from 10% to 98% B was applied over 3 min, maintained up to 6 min, and returned to the initial conditions, with a total run time of 8 min. Detection was performed in both positive and negative electrospray ionization (ESI^+/ESI^-) modes at a capillary voltage of 3.0 kV over a scan range of *m/z* 100–1000. Samples were filtered through a 0.22 µm membrane filter prior to injection. Phytoconstituents were tentatively identified based on their retention times, molecular ion (*m/z*) values, and comparison with published literature.

2.2. Computational studies

2.2.1. Compound Collection and Database Preparation:

Phytoconstituents reported in *Chenopodium album* were collected from published literature and curated databases, including IMPPAT (https://cb.imsc.res.in/imppat/) [22], PubMed, Scopus, and Web of Science.

2.2.2. Drug-Likeness Prediction:

SMILES structures of selected *Chenopodium album* phytoconstituents were retrieved from the PubChem database and evaluated for drug-likeness using the MolSoft online tool based on predicted physicochemical properties [23]. **(Supplementary table -T1**)

2.2.3. Network Pharmacology

The phytoconstituents of *Chenopodium album* were evaluated for their potential anti-epileptic mechanisms using network pharmacology. The chemical structures of the compounds were submitted to the SwissTargetPrediction platform to identify human protein targets [24,25].

Epilepsy-related genes were retrieved from the MalaCards database, prioritizing those with higher relevance scores. The intersection between compound and disease-associated genes was determined and visualized using a Venn diagram [26, 27].

These common targets were analyzed through DAVID Bioinformatics Resources to perform enrichment analysis. Gene Ontology (GO) classification was applied to group the targets into Biological Processes (BP), Molecular Functions (MF), and Cellular Components (CC). Kyoto Encyclopedia of Genes and Genomes (KEGG) pathway enrichment analysis was conducted to highlight the signaling pathways associated with these overlapping targets. Pathways with an adjusted p-value threshold of ≤ 0.05 were considered significant, and the most enriched ones were selected for graphical representation [28].

A protein–protein interaction (PPI) network was constructed using the STRING database for functional relationships among these targets [29].The network data were exported in .tsv format and imported into Cytoscape (version 3.10.0) for visualization. Hub genes were identified using the CytoHubba plugin based on degree score and betweenness centrality [30].The resulting interaction network illustrated the connections between compounds and targets, where nodes represented proteins or phytoconstituents and edges denoted their interactions [29, 30, 31, 32].

2.2.4. Molecular Docking

Molecular docking studies were performed to evaluate the binding interactions of the selected phytochemical ligands with the target protein. Three-dimensional structures of the selected phytochemical ligands were retrieved from the PubChem database or prepared using the LigPrep module of Schrödinger Suite Release 2024-4 (Schrödinger LLC, New York, NY, USA). LigPrep was used to generate ionization states, stereoisomers, and energetically favourable conformations. Geometry optimization and energy minimization were performed using the OPLS3e force field to obtain stable ligand conformations suitable for docking.

The crystal structure of STAT3 (PDB ID: 6NJS) was retrieved from the Protein Data Bank and prepared using the Protein Preparation Wizard in Schrödinger Suite Release 2024-4. During protein preparation, co-crystallized ligands, water molecules, and non-essential heteroatoms were removed, hydrogen atoms were added, bond orders were assigned, and the structure was energy-minimized using the OPLS3e force field. A receptor grid was generated around the active site based on the co-crystallized ligand using the Receptor Grid Generation module. Molecular docking was performed using the Glide Standard Precision (SP) docking protocol with default parameters.

The docking score (GlideScore) was used to rank ligand binding affinity, and the binding pose with the lowest docking score was selected for further analysis [33, 34].

2.2.5. Molecular Dynamics

The stability and conformational dynamics of the docked protein–ligand complex was evaluated using molecular dynamics (MD) simulations with Desmond (version 5.9) under the academic license from D. E. Shaw Research. The complex was embedded in an orthorhombic simulation box and solvated with the TIP3P water model, ensuring a minimum distance of 10 Å between the solute and the box boundaries. System neutrality was achieved by adding counterions (Na^+ and Cl^-), and atomic interactions were described using the OPLS force field. Energy minimisation using the OPLS-2005 force field was performed to eliminate unfavourable steric contacts and optimise the geometry. Equilibration was conducted under the NVT ensemble at 10 K using the Berendsen thermostat. A 100 ns production run was then performed under NPT conditions at 300 K and 1 atm. Temperature was controlled with the Nosé–Hoover chain thermostat, while pressure was maintained using the Martyna–Tobias–Klein barostat. Relaxation intervals of 20 ps were applied throughout the simulation to ensure system stability. Following the simulation, trajectory analyses were carried out using the Simulation Interaction Diagram module to assess structural stability, flexibility, and interaction behaviour of the protein–ligand complex [35, 36].

2.2.6. MMGBSA

The binding affinity of the ligand toward the target protein was assessed using the Molecular Mechanics/Generalized Born Surface Area (MM-GBSA) approach implemented in the Maestro Schrödinger Suite (version 12.3). Calculations were performed with the OPLS-2005 force field in combination with the VSGB 2.0 implicit solvent model.

The binding free energy (ΔG_{bind})was estimated using the equation:

$$\Delta G_{\text{bind}} = G_{\text{complex}} - (G_{\text{protein}} + G_{\text{ligand}})$$

where G_{complex}represents the total energy of the protein–ligand complex, including bonded and non-bonded interactions, while $G_{\text{protein}}$and G_{ligand}correspond to the energies of the isolated protein and ligand, respectively. This computational framework provided a quantitative measure of binding strength, offering insights into the stability and interaction efficiency of the protein–ligand complex [37, 38].

2.2.7. Post-Dynamic Analysis

Trajectory analysis was performed using computational tools implemented in Python to examine the conformational dynamics of the ligand-bound protein complex over the simulation. Principal Component Analysis (PCA) was applied to the covariance matrix derived from backbone atomic fluctuations, enabling identification of dominant collective motions. Eigenvalues and eigenvectors obtained from the covariance matrix were used for principal component analysis to identify the dominant conformational transitions. Backbone Cα atoms were employed to construct the Dynamic Cross-Correlation Matrix (DCCM) for analyzing residue motion correlations. Residue positional fluctuations were used to calculate cross-correlation coefficients, and the resulting heatmaps highlighted regions exhibiting correlated or anti-correlated motions. The first two principal components (PC1 and PC2) were selected as reaction coordinates to construct the Free Energy Landscape (FEL). The Boltzmann distribution was applied to calculate the free energy values, allowing visualization of energetically favourable conformations and identification of low-energy structural minima. This integrated approach provided a detailed understanding of the stability, flexibility, and dynamic properties of the protein–ligand complex across the simulation trajectory [39, 40].

2.2.8. The absorption, distribution, metabolism, excretion, and toxicity (ADMET) analysis

Among the phytoconstituents that satisfied the preliminary MolSoft drug-likeness criteria, the ten highest-ranked compounds based on molecular docking were selected for subsequent ADMET evaluation, along with the standard drug, were evaluated using the pkCSM platform (https://biosig.lab.uq.edu.au/pkcsm/), a graph-based computational platform for pharmacokinetic and toxicity prediction. The Canonical SMILES for each compound were obtained from the PubChem database and submitted individually to the pkCSM server. Compounds were examined for intestinal absorption, Caco-2 permeability, penetration across the blood–brain barrier (BBB), interactions with cytochrome P450 enzymes (CYP3A4 and CYP1A2) inhibition, and toxicity parameters such as AMES mutagenicity and hepatotoxicity, were predicted. The predicted ADMET profiles were summarized and compared in tabular form to assess pharmacokinetic behavior and toxicity profiles of the selected phytoconstituents [41].

2.3. Animal Ethics and Experimental Care

Swiss albino male mice weighing 25–30 gm were obtained from a CPCSEA-registered breeder (Reg. No. 2138/PO/RcBiBt/S/21/CPCSEA) and housed at the animal facility of Visveswarapura

Institute of Pharmaceutical Sciences under standard laboratory conditions (23 ± 2 °C, 50 ± 5% RH, 12 h light/dark cycle). The study protocol received ethical approval from the Institutional Animal Ethics Committee (IAEC), Visveswarapura Institute of Pharmaceutical Sciences (VIPS) (Project No. VIPS/IAEC/27-04-2024/25 AKV; Ref. No. VIPS/71/2024-25), Animal handling and experimental procedures adhered to the CPCSEA guidelines and international ethical standards.

2.4. Dose Selection:

Dose selection was guided by previously reported acute toxicity studies, which indicate that aqueous, ethanolic, and methanolic extracts of *Chenopodium album* are safe up to 2000 mg/kg without producing observable toxic effects [42, 43]. Based on these results, appropriate dose levels were chosen for the current investigation.

2.5. Chemicals and Experimental Reagents

Pentylenetetrazole (PTZ) was purchased from Sigma Aldrich (USA), and ethosuximide was obtained from Esjay Pharma Pvt. Ltd. (Tamil Nadu, India). Additional chemicals and reagents were of analytical grade and procured from Visveswarapura Institute of Pharmaceutical Sciences, Bengaluru.

2.6. Anticonvulsant Activity in PTZ-Induced Seizure Model

The pentylenetetrazole (PTZ) model serves as a standard experimental approach for the evaluation of seizure susceptibility and the assessment of potential anticonvulsant agents. PTZ acts as an antagonist at the $GABA_A$ receptor, resulting in reduced inhibitory neurotransmission and the induction of clonic or myoclonic seizures in rodents [44]. Repeated administration of sub convulsive doses of PTZ can lead to kindling, which reflects the progressive nature of epilepsy [45]. Due to its similarity to human myoclonic and absence seizures, this model is considered a reliable and widely accepted tool in experimental pharmacology [18].

A dose of 50 mg/kg (i.p.), previously optimized in our laboratory for consistent seizure induction [46], was used in the present study. Healthy adult male Swiss albino mice weighing 25–30 g were randomly allocated into five experimental groups, each comprising six animals. The control group (Group I) received distilled water orally, whereas Group II was administered the reference antiepileptic drug ethosuximide (150 mg/kg, p.o.). Groups III, IV, and V received the methanolic extract of *Chenopodium album* orally at doses of 100, 200, and 400 mg/kg, respectively.

On day 14, pentylenetetrazole (PTZ; 50 mg/kg, i.p.) was administered one hour after the respective treatments to induce seizures. Following PTZ injection, each animal was monitored for 30 min to

record the onset of convulsions, seizure duration, the number of animals exhibiting seizures, and mortality. Seizure intensity was assessed according to the modified Racine scoring system (score 0–6). The dose demonstrating the greatest anticonvulsant activity was subsequently selected for further investigation.

2.6.1. Evaluation of Combined Treatment

Thirty six Male Swiss albino mice with body weights ranging from 25 to 30 g were randomly assigned to the experimental groups, with each group comprising six animals. Animals in the control group were given distilled water (10 mL/kg) orally, whereas Ethosuximide (150 mg/kg, p.o.) was orally administered to the standard group for 14 consecutive days. The methanolic extract of *Chenopodium album* (400 mg/kg, p.o.) was provided to the treatment group for 14 consecutive days. Three additional groups received combinations of *C. album* extract together with ethosuximide in different ratios (50:50, 25:75, and 75:25). On day 14, seizures were induced using PTZ (50 mg/kg, i.p.) one hour after the final treatment. Seizure latency and duration were recorded, while seizure severity was assessed using the modified Racine scale (0–6)

2.6.2. Statistical Analysis

Results are presented as mean ± SEM (n = 6). Data were analyzed using one-way ANOVA followed by Dunnett's post hoc test for comparison with the control group. Statistical significance was defined by P values of <0.05, <0.01, and <0.001, whereas P values >0.05 indicated no significant difference. Seizure characteristics were evaluated by recording latency and duration, while behavioral manifestations were assigned Racine scores to determine seizure severity.

3. Results

3.1. Phytoconstituents Identification and Drug-Likeness Evaluation

Twenty-seven phytoconstituents derived from *Chenopodium album* were assessed for drug-likeness using Lipinski's Rule of Five. All compounds complied with the recommended physicochemical criteria, indicating favorable drug-like characteristics and suitability for further computational analysis. Ethosuximide (PubChem CID: 3307) was included as the reference compound for comparative evaluation.

3.2. Extract Yield and Phytochemical Analysis

Methanolic extraction (99.8%) of *Chenopodium album* leaves yielded 32.72% (w/w) of crude extract. Preliminary phytochemical screening revealed the presence of flavonoids, phenolic

compounds, alkaloids, triterpenoids, saponins, tannins, steroids, coumarins, carbohydrates, and cardiac glycosides.

Table 1: Preliminary Identification of Phytochemical Constituents

Phytochemical Class	Observation
Phenols	Detected
Flavonoids	Detected
Tannins	Detected
Coumarin	Detected
Chlorogenic acid	Detected
Alkaloids	Detected
Glycosides	Detected
Saponins	Detected
Terpene	Detected
Steroids	Detected
Protein	Detected
Amino Acids	Detected
Monosaccharides	Detected
Reducing sugar	Detected
Non reducing polysaccharide	Detected
Fats and essential oil	Detected

3.3. LC-MS Profile: LC–MS profiling of the methanolic extract of *Chenopodium album* identified the presence of multiple bioactive phytoconstituents, including phenolic acids, flavonoids, terpenoids, and other low-molecular-weight compounds. The detailed phytochemical profile, retention times, and molecular weights are summarized in **Table 2**, with **Figures 1-3** display representative LC–MS spectra.

Figure 1:

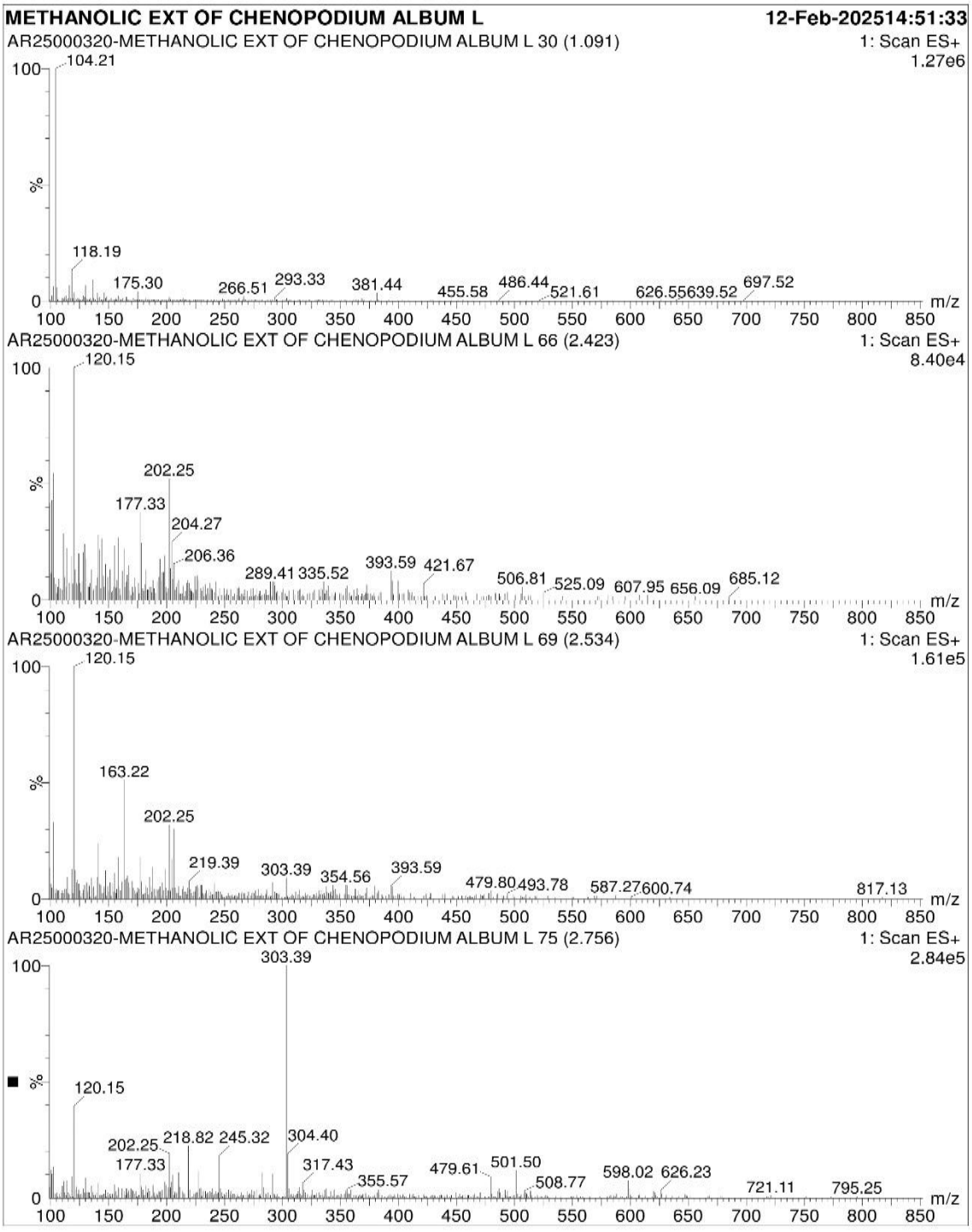
METHANOLIC EXT OF CHENOPODIUM ALBUM L
12-Feb-202514:51:33
AR25000320-METHANOLIC EXT OF CHENOPODIUM ALBUM L 30 (1.091)
1: Scan ES+
1.27e6
104.21
118.19
175.30
266.51
293.33
381.44
455.58
486.44
521.61
626.55639.52
697.52
AR25000320-METHANOLIC EXT OF CHENOPODIUM ALBUM L 66 (2.423)
1: Scan ES+
8.40e4
120.15
202.25
177.33
204.27
206.36
289.41 335.52
393.59
421.67
506.81
525.09
607.95
656.09
685.12
AR25000320-METHANOLIC EXT OF CHENOPODIUM ALBUM L 69 (2.534)
1: Scan ES+
1.61e5
120.15
163.22
202.25
219.39
303.39
354.56
393.59
479.80
493.78
587.27
600.74
817.13
AR25000320-METHANOLIC EXT OF CHENOPODIUM ALBUM L 75 (2.756)
1: Scan ES+
2.84e5
303.39
120.15
202.25
177.33
218.82
245.32
304.40
317.43
355.57
479.61
501.50
508.77
598.02
626.23
721.11
795.25
%
m/z
100
150
200
250
300
350
400
450
500
550
600
650
700
750
800
850
0

Figure 2:

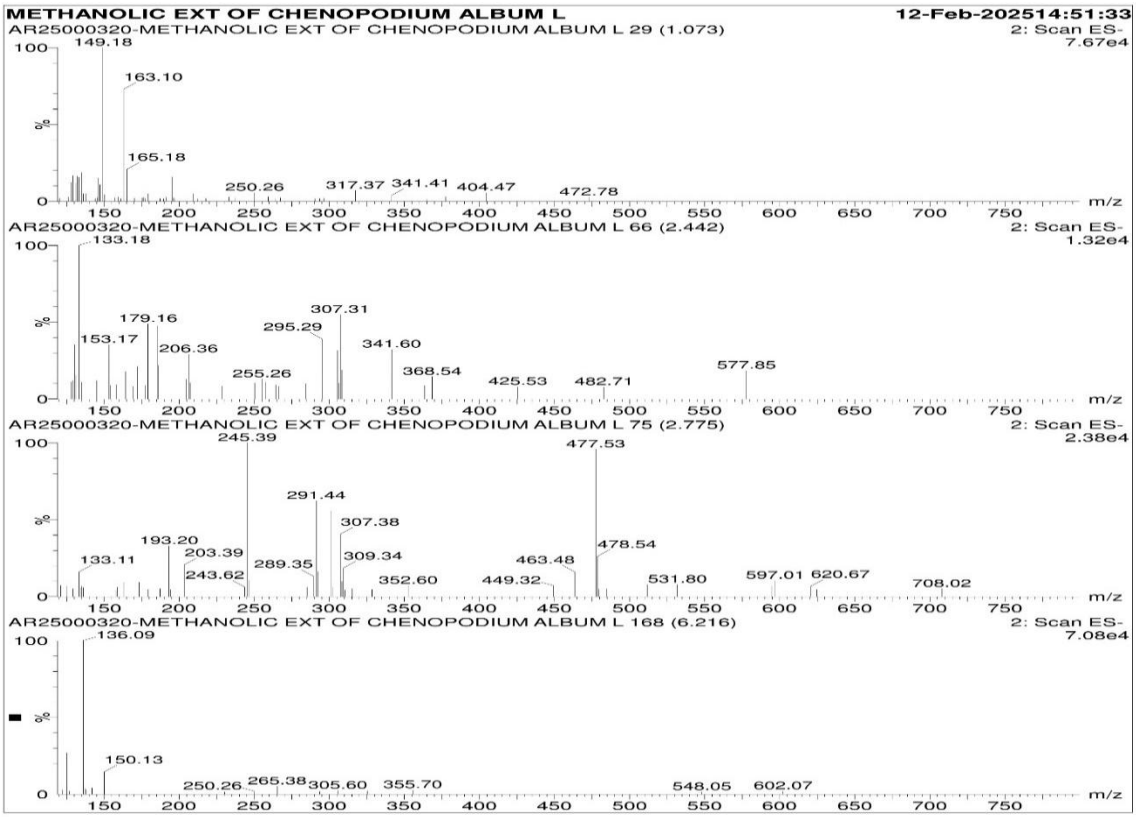

Figure 3:

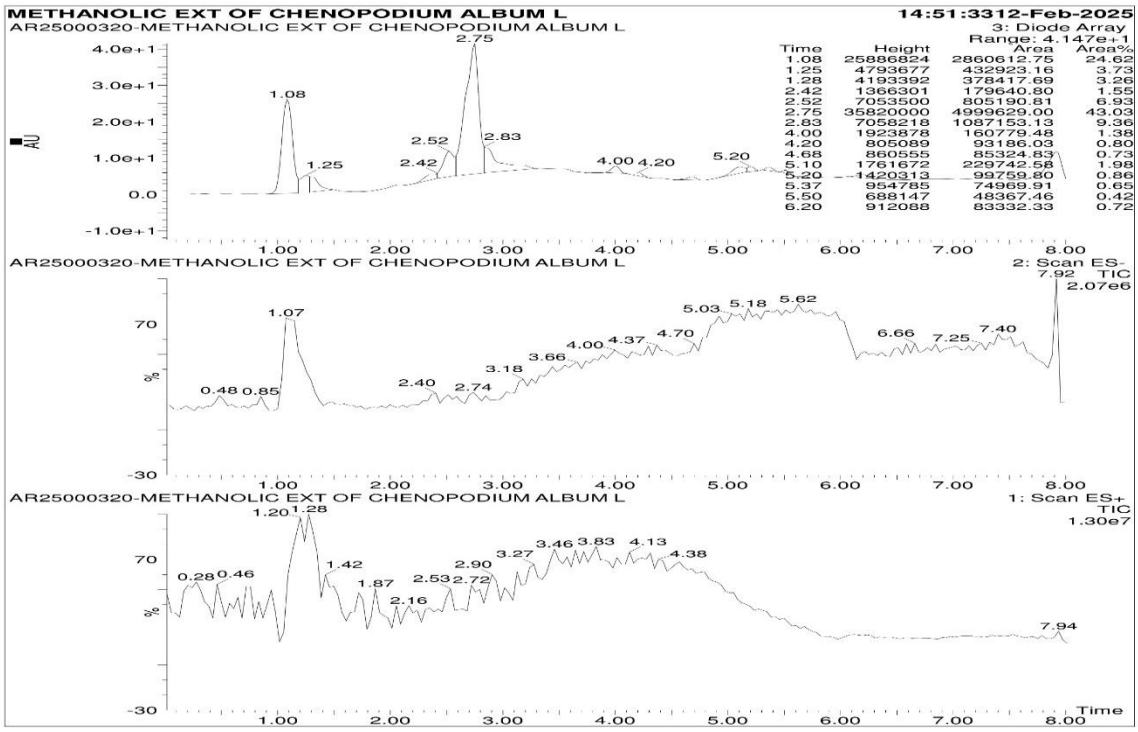

Table 2: LC–MS-Based Phytochemical Analysis of the Methanolic Extract Prepared from *Chenopodium album* L. Leaves

Sample	Phytoconstituents	Molecular Formula	Molecular Weight(g/mol)	Retention Time
Methanolic extract of *Chenopodium album L*	Cinnamic acid	$C_9H_8O_2$	148.05	1.073
	Thymol	$C_{10}H_{14}O$	150.1	1.073
	m-coumaric acid	$C_9H_8O_3$	164.05	1.073
	4-hydroxycinnamic acid	$C_9H_8O_3$	164.05	1.073
	Vanillin	$C_8H_8O_3$	152.05	2.442
	Linalool	$C_{10}H_{18}O$	154.14	2.442
	Protocatechuic acid	$C_7H_6O_4$	154.03	2.442
	Caffeic acid	$C_9H_8O_4$	180.04	2.442
	Acetyl eugenol	$C_{12}H_{14}O_3$	206.09	2.442
	Gallocatechin	$C_{15}H_{14}O_7$	306.07	2.442
	Lupeol	$C_{30}H_{50}O$	426.39	2.442
	Leucine	$C_6H_{13}NO_2$	131.09	2.775
	p-cymene	$C_{10}H_{14}$	134.11	2.775
	Scopoletin	$C_{10}H_8O_4$	192.04	2.775
	Ferulic acid	$C_{10}H_{10}O_4$	194.06	2.775
	Limonene	$C_{10}H_{16}$	136.13	6.216
	α-pinene	$C_{10}H_{16}$	136.13	6.216
	β-pinene	$C_{10}H_{16}$	136.13	6.216
	Camphene	$C_{10}H_{16}$	136.13	6.216
	Choline	$C_5H_{14}NO$	104.11	1.091
	Betaine	$C_5H_{11}NO_2$	117.08	1.091
	Oleanolic acid	$C_{30}H_{48}O_3$	456.36	1.091
	Ascorbic acid	$C_6H_8O_6$	176.03	2.423
	Ethyl cinnamate	$C_{11}H_{12}O_2$	176.08	2.423
	Methyl ferulate	$C_{11}H_{12}O_4$	208.07	2.423
	Elemicin	$C_{12}H_{16}O_3$	208.11	2.423
	Quercetin	$C_{15}H_{10}O_7$	302.23	2.534

Table 3: List of Commercial and Plant-Derived Compounds Retrieved from the PubChem Database

Commercial compounds					
SL NO.	**Commercial compounds**	**PubChem CID**	**2D Structures**	**3D Structures**	**Type of Compounds**
1	Ethosuximide	3291	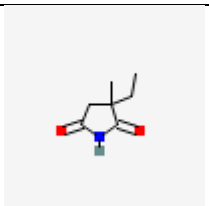		Commercial
Natural compounds from *Chenopodium album L.*					
2	Cinnamic acid	444539	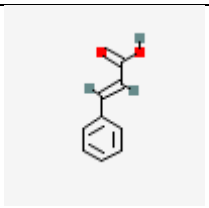	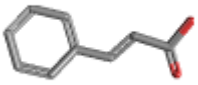	Phenolic
3	Thymol	6989	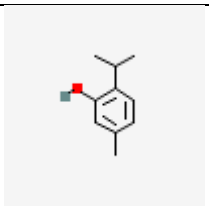		Phenolic
4	*m*-coumaric acid	637541	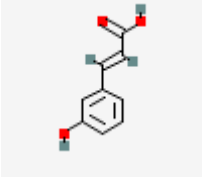	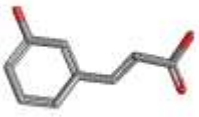	Phenolic
5	4-hydroxycinnamic acid	322	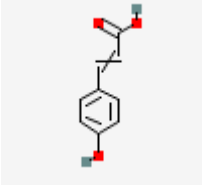		Phenolic
6	Vanillin	1183	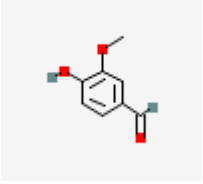		Phenolic

7	Linalool	6549	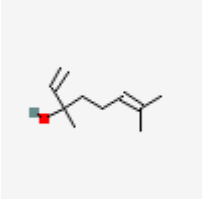		Terpenoid
8	Protocatechuic acid	72	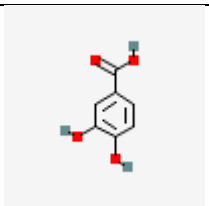		Phenolic
9	Caffeic acid	689043	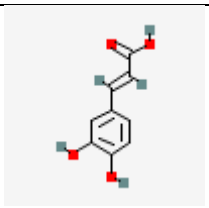	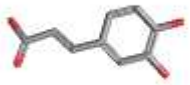	Phenolic
10	Acetyl eugenol	7136	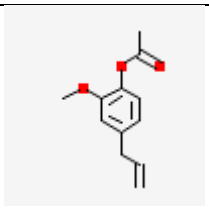	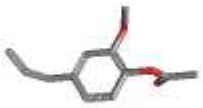	Phenolic
11	Gallocatechin	65084	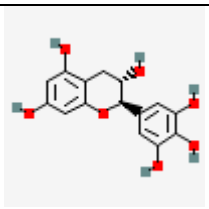		Flavonoid
12	Lupeol	259846	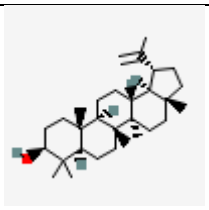	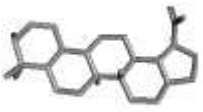	Terpenoid
13	Leucine	6106	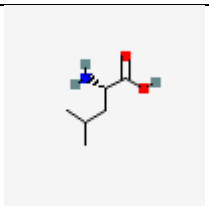		Essential amino acid

14	*p*-cymene	7463	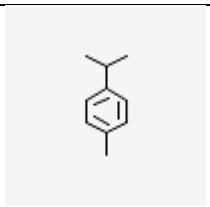		Terpenoid
15	Scopoletin	5280460	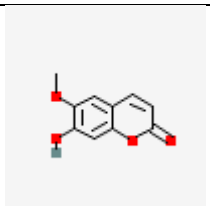	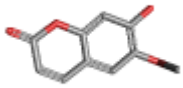	Phenolic
16	Ferulic acid	445858	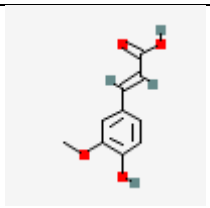	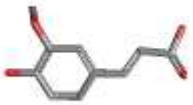	Phenolic
17	Limonene	22311			Terpenoid
18	α-pinene	6654			Terpenoid
19	β-pinene	14896	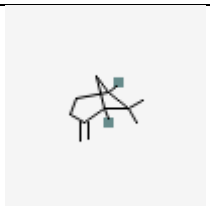		Terpenoid
20	Camphene	6616	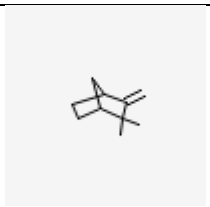		Terpenoid

21	Choline	305	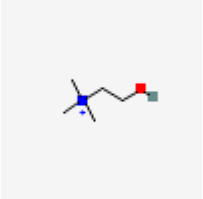		Quaternary ammonium compound
22	Betaine	247	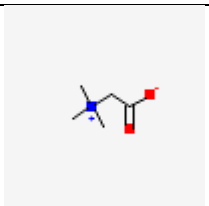		Quaternary ammonium compound
23	Oleanolic acid	10494	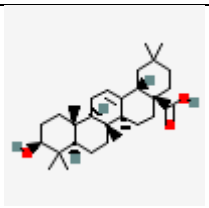	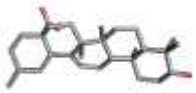	Terpenoid
24	Ascorbic acid	54670067	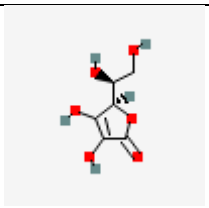		Water-soluble vitamin (Vitamin C)
25	Ethyl cinnamate	637758	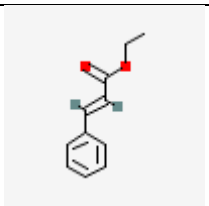	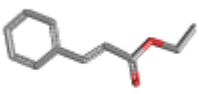	Phenolic
26	Methyl ferulate	5357283	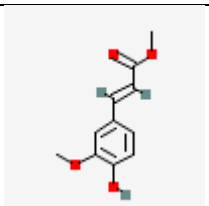	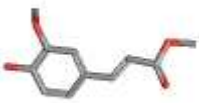	Phenolic
27	Elemicin	10248	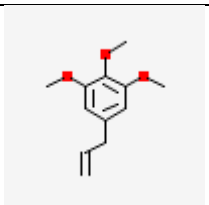		Phenolic

28	Quercetin	5280343	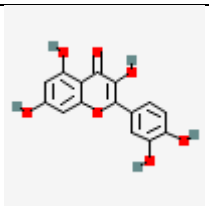		Flavonoid

3.4. Computational results

3.4.1. Network Pharmacology

Prediction of Targets and Common Target Analysis

A total of 27 phytoconstituents identified from *Chenopodium album* were subjected to target prediction using the SwissTargetPrediction tool, resulting in the identification of 712 putative human protein targets after removal of duplicates. Epilepsy-related genes were obtained from the GeneCards database, yielding 10,045 disease-related targets. Comparative analysis between the phytoconstituent-associated targets and epilepsy-related genes identified 541 common targets. It provided molecular targets involved in pathophysiology of epilepsy. The overlap between compound targets and epilepsy-associated genes is illustrated in **Figure 4**.

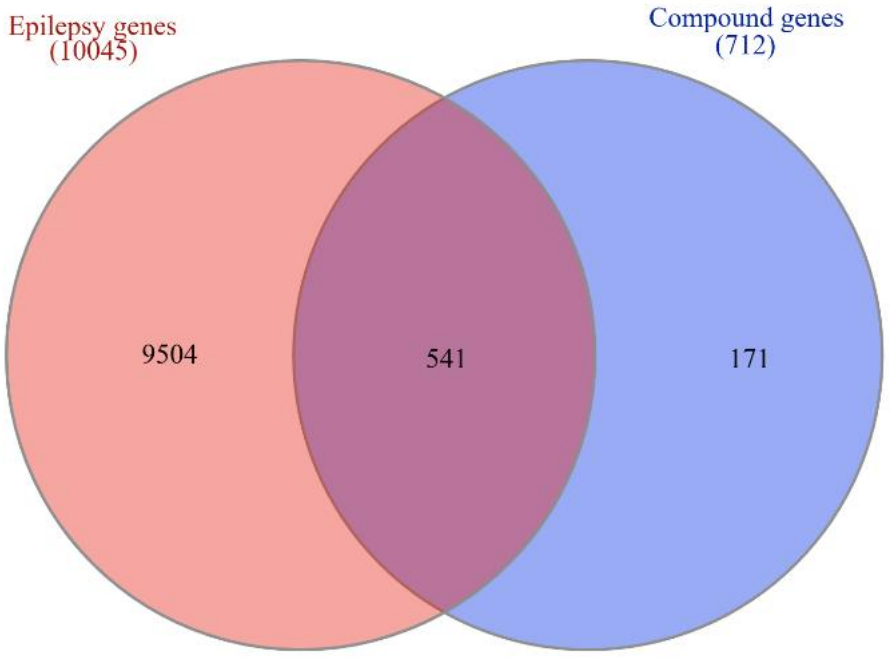

Figure 4. Disease and designed compound overlapping targets

3.4.2. Protein–Protein Interaction (PPI) Analysis

The functional associations among the 541 common targets were examined by a Protein–protein interaction (PPI) analysis was performed with the STRING database. The resulting network revealed extensive interactions between the proteins, indicating that the identified targets participate in highly coordinated biological processes and signalling pathways associated with epilepsy. Such interactions highlight the multi-target therapeutic potential of *C. album* phytoconstituents in modulating epilepsy-related biological pathways. The generated PPI network is presented in **Figure 5**.

3.4.3. Identification of the Top 10 Hub Genes Using Network Pharmacology

Network topology analysis was conducted to identify highly connected hub genes according to node degree. The degree score represents the total number of proteins directly connected to a given protein within the interaction network, thereby indicating its potential biological importance. The analysis identified the ten highest-ranked hub genes, namely STAT3, EGFR, HSP90AA1, AKT1, CTNNB1, SRC, IL6, ESR1, EP300, and BCL2. Among these, STAT3 exhibited the highest degree score (86), followed by EGFR (83), HSP90AA1 (82), and AKT1 (82), suggesting their central roles in regulating epilepsy-associated signalling networks. The degree scores of the top ten hub genes are summarized in **Table 4**, while their interaction network is depicted in **Figure 6**.

Table 4. Top 10 Hub genes ranked by degree score

Rank	**1**	**2**	**3**	**4**	**5**	**6**	**7**	**8**	**9**	**10**
Gene name	STAT3	EGFR	HSP90AA1	AKT1	CTNNB1	SRC	IL6	ESR1	EP300	BCL2
Degree Score	86	83	82	82	81	80	70	64	63	61

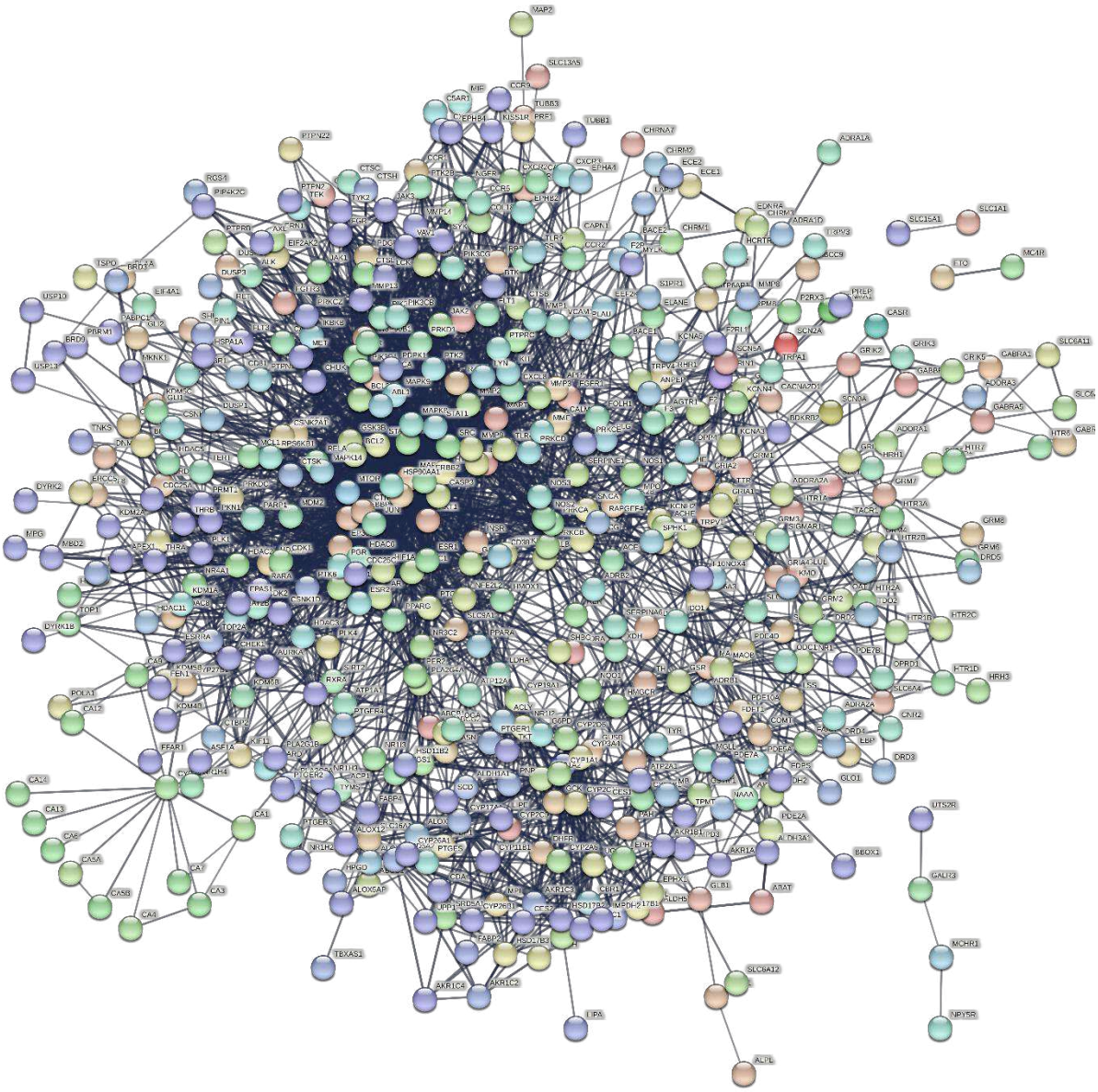

Figure 5. Network of Protein–Protein Interactions

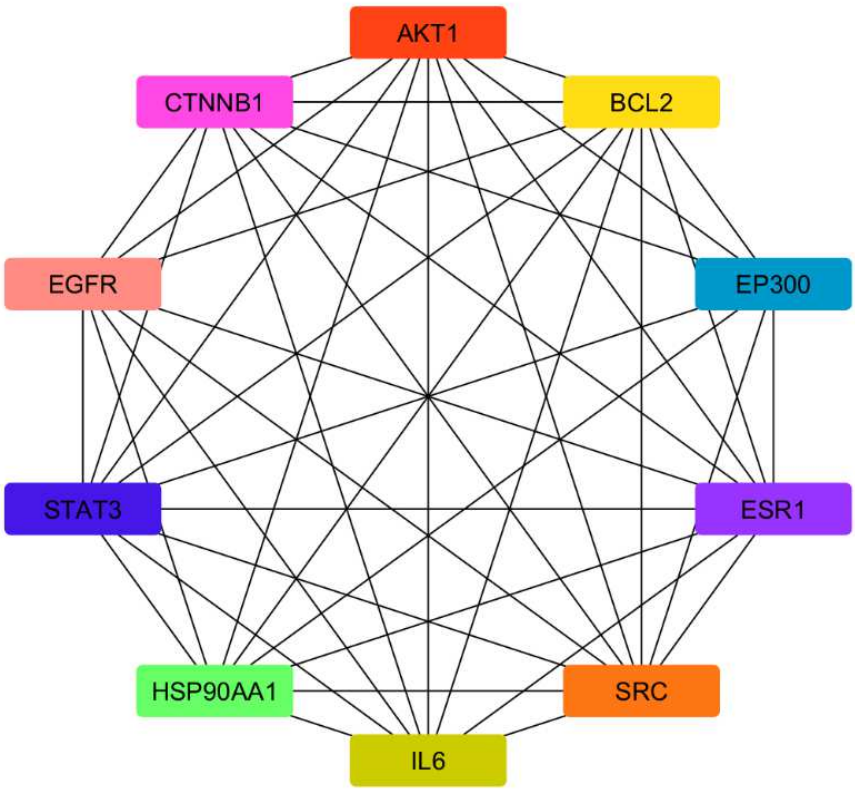

Figure 6. Top 10-ranked genes network diagram

3.4.4. Compound-Target -Pathway network

The 541 shared targets were subjected to functional enrichment analysis using ShinyGO to identify significantly enriched biological pathways. The enriched pathways along with the respective statistical parameters are presented in **Table 5**. Among the identified pathways, EGFR tyrosine kinase inhibitor resistance demonstrated the highest fold enrichment value (16.77), indicating a strong association with the common targets. This finding suggests that modulation of EGFR-mediated signalling may contribute to the therapeutic effects of *C. album* phytoconstituents in epilepsy. Based on the enriched pathway and its associated targets and compounds, a Compound-Target-Pathway (C-T-P) network was constructed using Cytoscape. The network provides a comprehensive visualization of the biological interactions among bioactive phytoconstituents, their molecular targets, and the EGFR pathway involved in epilepsy, supporting the multi-component and multi-target mode of action of *C. album* (**Figure 7**).

Table 5:

Enrichment FDR	nGenes	Pathway Genes	Fold Enrichment	Pathway
1.08E-28	31	79	16.77675912	Path:hsa01521 EGFR tyrosine kinase inhibitor resistance
2.17E-29	34	97	14.98582474	Path:hsa04750 Inflammatory mediator reg. of TRP channels
3.87E-29	34	99	14.68308081	Path:hsa04933 AGE-RAGE signaling pathway in diabetic complications
3.05E-28	33	97	14.54506519	Path:hsa05215 Prostate cancer
2.25E-31	37	109	14.51271587	Path:hsa04066 HIF-1 signaling pathway
3.44E-26	33	111	12.71055246	Path:hsa04726 Serotonergic synapse
1.30E-27	38	147	11.05197079	Path:hsa04072 Phospholipase D signaling pathway
5.11E-26	36	141	10.91583229	Path:hsa05418 Fluid shear stress and atherosclerosis
5.51E-27	39	163	10.22940725	Path:hsa05161 Hepatitis B

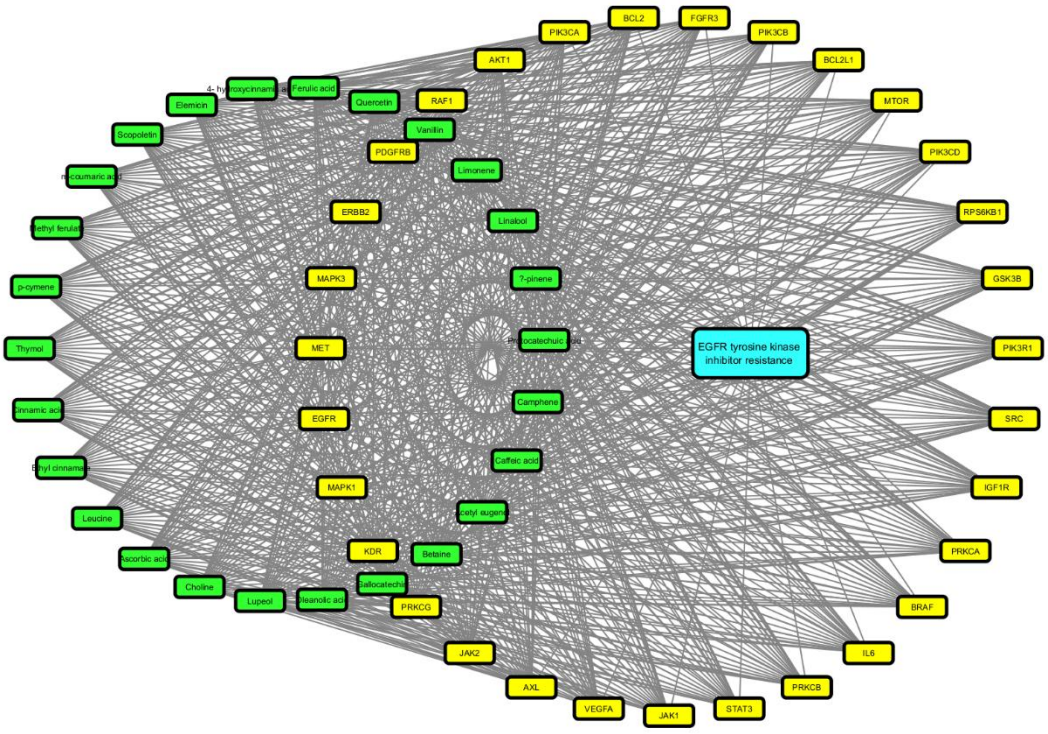

Figure 7: Compound-Target -Pathway (C-T-C) network

3.4.5. Role of the top 10 genes in epilepsy

The predicted hub genes have been widely implicated in the pathogenesis and progression of epilepsy through their involvement in neuroinflammation, neuronal survival, synaptic plasticity, and signal transduction pathways. STAT3 and IL6 are key mediators of inflammatory signalling and have been associated with seizure-induced neuroinflammation and neuronal damage. EGFR, AKT1, and SRC participate in cellular signalling pathways that regulate neuronal growth, survival, and excitability, which are frequently altered during epileptogenesis. HSP90AA1 functions as a molecular chaperone that stabilizes several signalling proteins involved in neuronal stress responses. CTNNB1 plays a critical role in Wnt/β-catenin signalling, which influences neuronal development and synaptic remodelling. ESR1 has been reported to modulate neuronal excitability through estrogen-mediated neuroprotective mechanisms, while EP300 acts as a transcriptional co-activator associated in the regulation of genes related to neuronal plasticity and memory formation. BCL2 contributes to neuronal survival by inhibiting apoptosis and protecting against seizure-induced cell death. These hub genes represent important molecular regulators of epilepsy and may serve as potential therapeutic targets through which *C. album* phytoconstituents exert their neuroprotective and anti-epileptic effects.

3.4.6. Gene Ontology (GO) Analysis

Functional enrichment based on Gene Ontology (GO) was conducted for the STAT3-associated overlapping targets to investigate their biological functions, cellular localization, and molecular activities as shown in **Figure 8**. In the Biological Process (BP) category, the enriched targets were predominantly associated with positive regulation of gene expression, negative regulation of apoptotic processes, and positive regulation of transcription by RNA polymerase II, cell proliferation, and DNA-templated transcription. Additional enrichment was observed in processes related to RNA polymerase II transcription, epidermal growth factor receptor signalling pathways, cell differentiation, and signal transduction. The analysis revealed that the identified targets are involved in regulating gene expression, cellular growth, survival, and signalling that contribute to neuronal function and pathological alterations associated with epilepsy.

Cellular Component (CC) analysis demonstrated that the targets were primarily located in the cytosol, nucleus, cytoplasm, and protein-containing complexes. Significant enrichment was also observed in the plasma membrane, nucleoplasm, transcription regulator complexes, perinuclear cytoplasmic region, and cell junctions. The distribution of targets across these cell ular

compartments suggests their involvement in intracellular signalling, transcriptional regulation, and intercellular communication required for neuronal activity and seizure development.

Within the Molecular Function (MF) category, the enriched targets were mainly associated with protein binding, which exhibited the highest enrichment count. Other significant functions included identical protein binding, protein phosphatase binding, enzyme binding, DNA-binding transcription factor binding, ubiquitin protein ligase binding, chromatin binding, ATP binding, and nucleotide binding. These molecular activities highlight the ability of the targets to participate in protein–protein interactions, signal transduction cascades, transcriptional regulation, and cellular energy-dependent processes.

3.4.7. Enrichment Analysis of KEGG Pathways

Several significantly enriched KEGG signaling pathways associated with the anti-epileptic potential of *Chenopodium album* were identified from the overlapping targets, as illustrated in **Figure 9.** Among the significantly enriched pathways, EGFR tyrosine kinase inhibitor resistance exhibited the highest enrichment score, indicating the prominent involvement of EGFR-mediated signaling in the identified target network. Dysregulation of EGFR signaling has been associated with neuroinflammation, neuronal survival, and abnormal cellular responses that contribute to epileptogenesis. Other pathways included the JAK–STAT signaling pathway, estrogen signaling pathway, and HIF-1 signaling pathway, that are known to regulate inflammatory responses, oxidative stress, neuronal protection, and synaptic plasticity in the central nervous system. Several disease-related pathways, including pathways in cancer, prostate cancer, proteoglycans in cancer, and chemical carcinogenesis–receptor activation, were also significantly enriched. Furthermore, enrichment of the Kaposi sarcoma-associated herpesvirus infection and Hepatitis B pathways reflects the participation of inflammatory and immune-regulatory signaling networks rather than direct disease relevance. The KEGG analysis demonstrates that the overlapping targets are enriched in pathways governing inflammation, cellular survival, transcriptional regulation, and signal transduction.

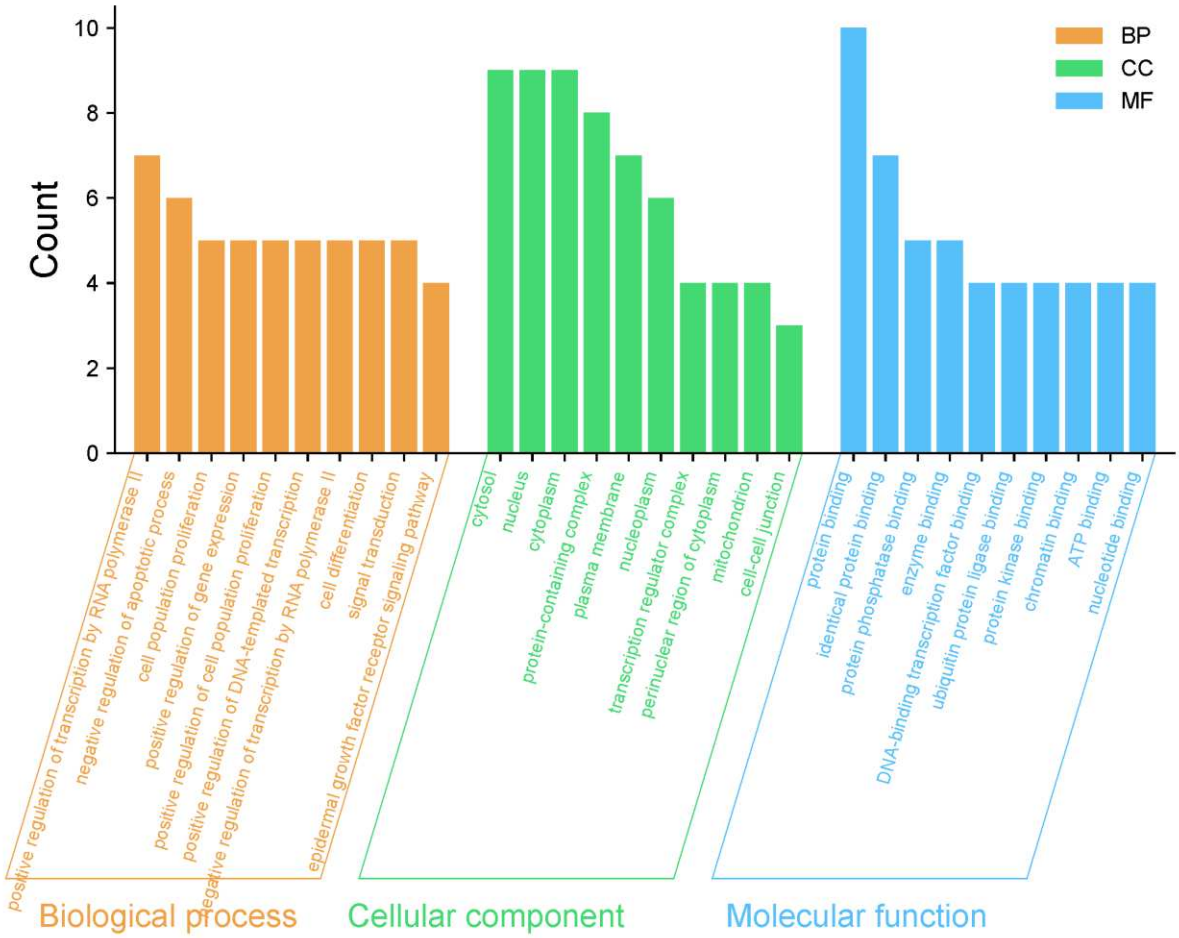

Figure 8. Gene Ontology (GO) enrichment results illustrating Biological Processes, Cellular Components, and Molecular Functions, represented in orange, green, and blue, respectively.

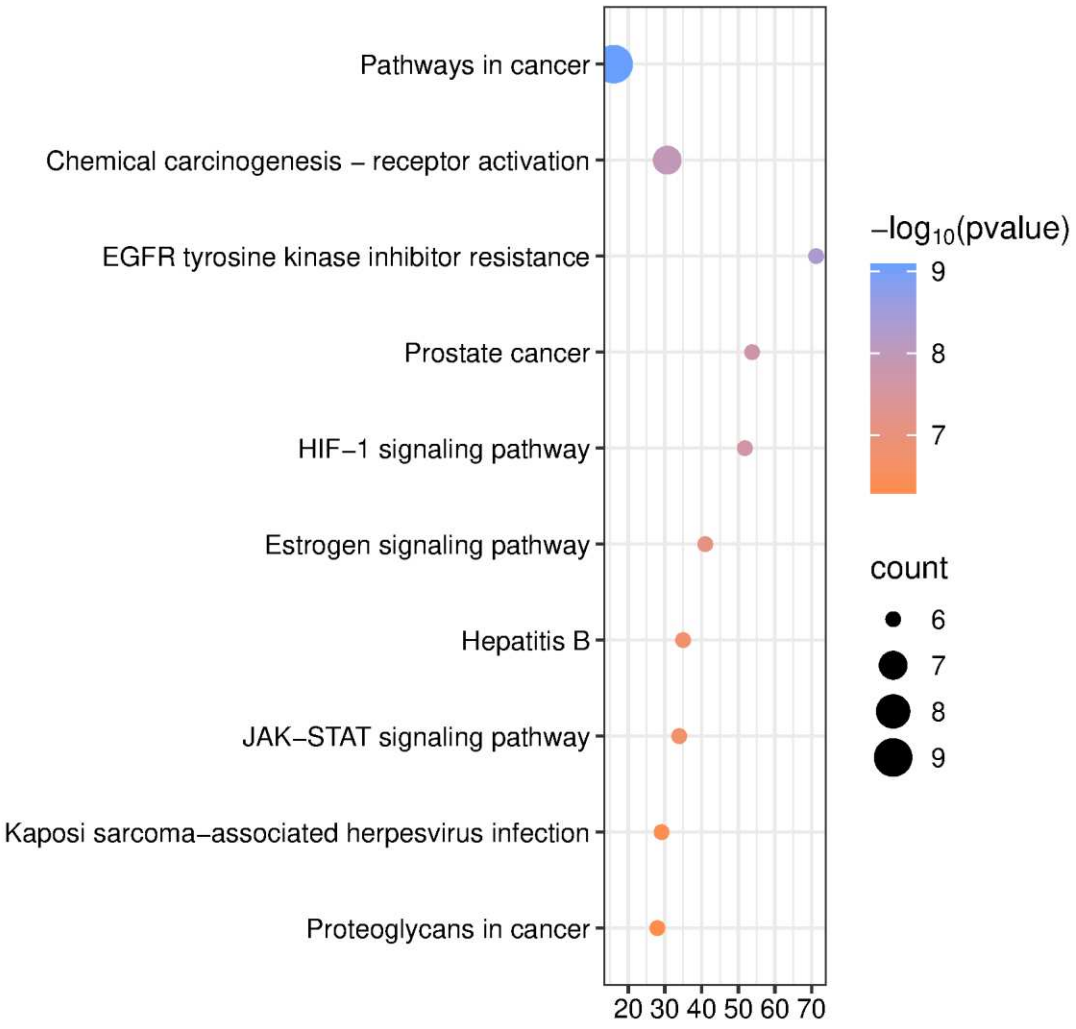

Figure 9. Enriched KEGG Pathways

3.4.8. Molecular Docking Analysis

Binding affinities and ligand–protein interaction profiles of the 26 ligands derived from the 27 phytoconstituents identified in *Chenopodium album* were evaluated through molecular docking analysis against the STAT3 protein. Since α-pinene and β-pinene were represented as a single ligand (Pinene), a total of 26 ligands were included in the docking study. **Table 6** presents the docking scores of all the evaluated ligands. Among them, quercetin demonstrated the strongest binding affinity, with a docking score of −4.53 kcal/mol, followed by scopoletin (−4.41 kcal/mol), gallocatechin (−4.31 kcal/mol), acetyl eugenol (−4.16 kcal/mol), 4-hydroxycinnamic acid (−4.13 kcal/mol), and thymol (−4.13 kcal/mol). The remaining ligands exhibited moderate to weak

binding affinities, with docking scores ranging from −4.09 to −1.52 kcal/mol. The superior docking score of quercetin suggests a stronger interaction with the STAT3 binding pocket than the other ligands, indicating its potential as a promising STAT3 inhibitor.

Quercetin, with the highest binding affinity, presented favourable interactions with the STAT3 target. The hydroxyl groups present on the flavonoid formed hydrogen-bonding interactions with Glu625, water-mediated interactions involving Lys626 and Ile628, carbonyl oxygen of the chromenone ring participated in polar interactions within the active site. These interactions contributed to the binding affinity observed for quercetin and stable accommodation within the STAT3 binding cavity.

The co-crystallized ligand exhibited strong hydrogen-bond interactions with Ala250, Asp261, and Gln511, indicating their role in ligand stabilization. Water-bridge interactions observed through Arg350, Cys251, and Pro333. The aromatic moieties of the ligand also contributed to hydrophobic interactions that enhanced binding stability.

Comparison of the binding modes, both quercetin and the co-crystal ligand established favourable interactions within the STAT3 binding pocket. While the co-crystal ligand formed a larger number of direct and water-mediated hydrogen bonds, quercetin achieved comparable stabilization. This suggests its potential to effectively bind STAT3 and modulate its biological activity. The 2D interaction image is provided in **Figure 10.**

Table 6. Summarizes the docking scores of all the identified phytoconstituents.

S.No	Compound name	Binding affinity (kcal/mol)
1	Quercetin	-4.53
2	Scopoletin	-4.41
3	Gallocatechin	-4.31
4	Acetyl eugenol	-4.16
5	4-Hydroxycinnamic acid	-4.13
6	Thymol	-4.13
7	Elemicin	-4.09
8	Protocatechuic acid	-4.09
9	Caffeic acid	-3.91
10	Betaine	-3.77
11	Ferulic acid	-3.75
12	Methyl ferulate	-3.68
13	m-Coumaric acid	-3.67
14	p-Cymene	-3.66

15	Leucine	-3.64
16	Ethyl cinnamate	-3.33
17	Cinnamic acid	-3.25
18	Ascorbic acid	-3.12
19	Oleanolic acid	-2.9
20	Limonene	-2.81
21	Choline	-2.64
22	Linalool	-1.87
23	Camphene	-1.62
24	Lupeol	-1.6
25	Pinene	-1.54
26	Vanillin	-1.52

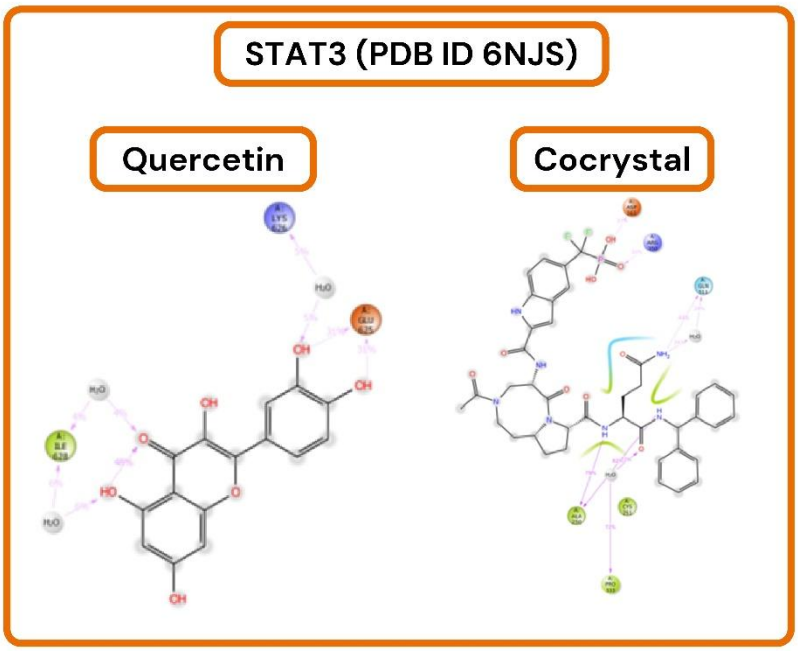

Figure 10. 2D representation of the quercetin and the cocrystal

3.4.9. Analysis of Molecular Dynamics Simulations

The quercetin–STAT3 complex underwent a 100 ns molecular dynamics (MD) simulation.to investigate its structural stability, conformational changes, and persistence of binding, with the co-crystallized ligand serving as the reference for comparison. Simulation trajectories were subsequently evaluated using Root Mean Square Deviation (RMSD), Root Mean Square Fluctuation (RMSF), protein–ligand interaction analysis, and ligand property analysis.

3.5. Root Mean Square Deviation (RMSD)

Structural stability of the STAT3–ligand complexes was examined by monitoring RMSD throughout the 100 ns molecular dynamics simulation (**Figure 11**). For the quercetin–STAT3 complex, the protein backbone exhibited an initial RMSD of approximately 2.4 Å, which increased to nearly 4.2 Å during the equilibration stage. Fluctuations were observed up to 20 ns, then remained within the range of 3.0–4.2 Å until ~60 ns. Later, the RMSD gradually decreased to around 3.0 Å by 75 ns and remained relatively stable between 3.0 and 3.8 Å till 100ns. The RMSD of quercetin initially remained low, fluctuating between 0.6 and 1.2 Å for nearly 45 ns, indicating a stable binding within the STAT3 binding pocket. Between 45 and 80 ns, the ligand displayed increased mobility, as indicated by RMSD values between 1.2 and 4.2 Å.suggesting conformational rearrangement within the binding site. Thereafter, the ligand RMSD gradually decreased and stabilized around 1.8 Å by 90ns, indicating retention of the ligand within the binding cavity.

For the STAT3 co-crystal complex, the protein RMSD began at approximately 2.0 Å and remained within 2.0–3.0 Å during the first 40 ns. A gradual increase was observed between 3.0 and 4.0 Å until the end of the simulation. The RMSD profile of the co-crystallized ligand increased from approximately 1.0 Å to 3.5–4.0 Å over the course of the simulation, reflecting structural rearrangements within the binding pocket. Overall, both complexes maintained structural stability throughout the simulation.

3.5.1. Analysis of Root Mean Square Fluctuation (RMSF)

RMSF analysis was conducted to evaluate residue-wise flexibility and local structural fluctuations during the simulation (**Figure 11**). In the quercetin–STAT3 complex, most protein residues displayed RMSF values below 5.6 Å, indicating limited flexibility and preservation of the overall protein architecture throughout the trajectory. The ligand atom fluctuations remained below 20 Å, suggesting that certain ligand atoms experienced mobility, the compound remained associated with the binding site. The STAT3 co-crystal complex exhibited low residue fluctuations, with most protein residues maintaining RMSF values below 4.0 Å. The co-crystal ligand demonstrated minimal atomic fluctuations, remaining below 4.0 Å throughout the simulation.

3.5.2. Protein–Ligand Interaction Assessment

Changes in conformational dynamics and structural compactness of quercetin and the co-crystallized ligand were evaluated using ligand property analysis (**Figure 12**).The quercetin–

STAT3 complex maintained stable hydrogen-bond interactions with Glu625, Asp676, and Glu681, exhibiting interaction fractions of approximately 0.70, 0.10, and 0.10, respectively. Lys626 interacted through hydrogen bonds, ionic interactions, hydrophobic contacts, and water-mediated bridges, with an interaction fraction of approximately 0.20. Ile628 formed hydrophobic contacts and water-bridge interactions with a similar interaction fraction. In the STAT3 co-crystal complex, strong hydrogen bond interactions were primarily observed with Ala250, Asp261, Gln511, and Leu260, exhibiting interaction fractions of approximately 1.75, 1.25, 1.25, and 0.75, respectively. Additional stabilization was provided through water-mediated interactions involving Asp261, Asp334, Arg335, Arg350, and Ser514, with interaction fractions ranging from 0.25 to 0.75.

3.5.3. Ligand Property Analysis

Ligand property profiles of quercetin and the co-crystallized ligand were examined to characterize their structural compactness and conformational dynamics (**Figure 12**). For quercetin, the radius of gyration (Rg) exhibited highly stable, fluctuating within the range of 3.72–3.82 Å throughout the 100 ns simulation, consistent with structural compactness. The molecular surface area (MolSA) exhibited values ranging from 52.5 to 57.5 Å², reflecting minimal changes in ligand geometry. The solvent-accessible surface area (SASA) values ranged from 200 to 300 Å² during the initial 45 ns of the simulation, followed by an increase to approximately 500 Å² before declining to nearly 300 Å² during the final stage of the simulation.The polar surface area (PSA) varied between 270 and 282 Å² throughout the trajectory, reflecting consistent exposure of polar functional groups.

However, the co-crystal ligand exhibited a larger and less compact structure, with an Rg value initially around 5.5 Å and subsequently stabilizing between 6.0 and 6.5 Å. The MolSA values ranged between 650 and 700 Å², while SASA fluctuated between 400 and 480 Å² during the simulation. The PSA remained relatively stable within the range of 340–375 Å².

These observations suggest that both ligands maintained structural integrity during the simulation. However, quercetin exhibited a compact and stable conformational profile while preserving favorable interactions with key STAT3 residues.

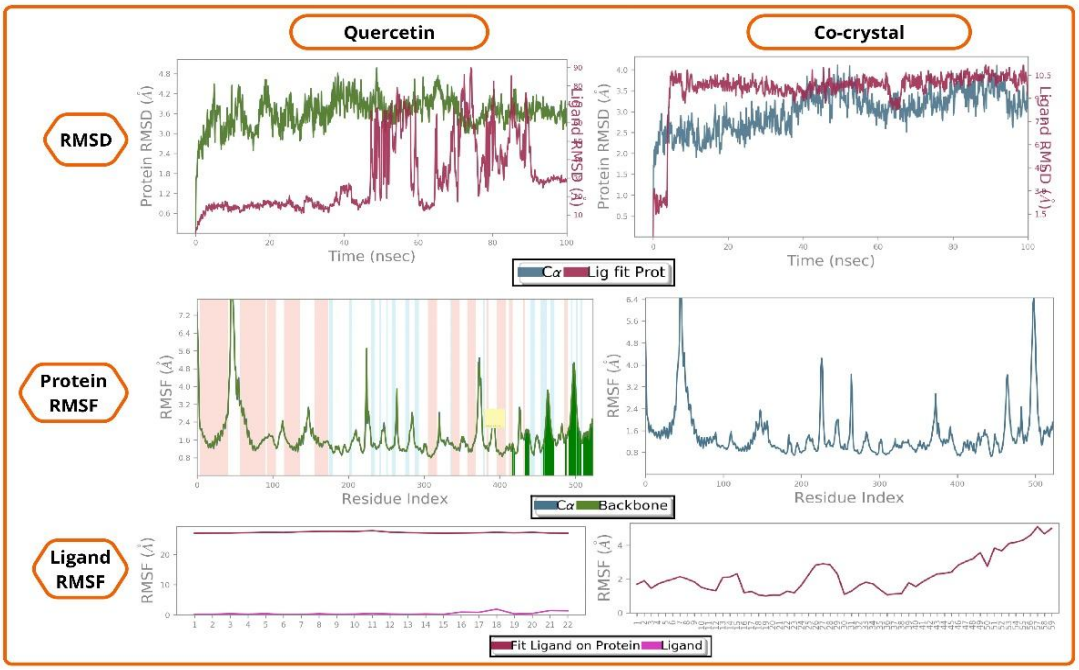

Figure 11: RMSD and RMSF plots of the quercetin and the cocrystal

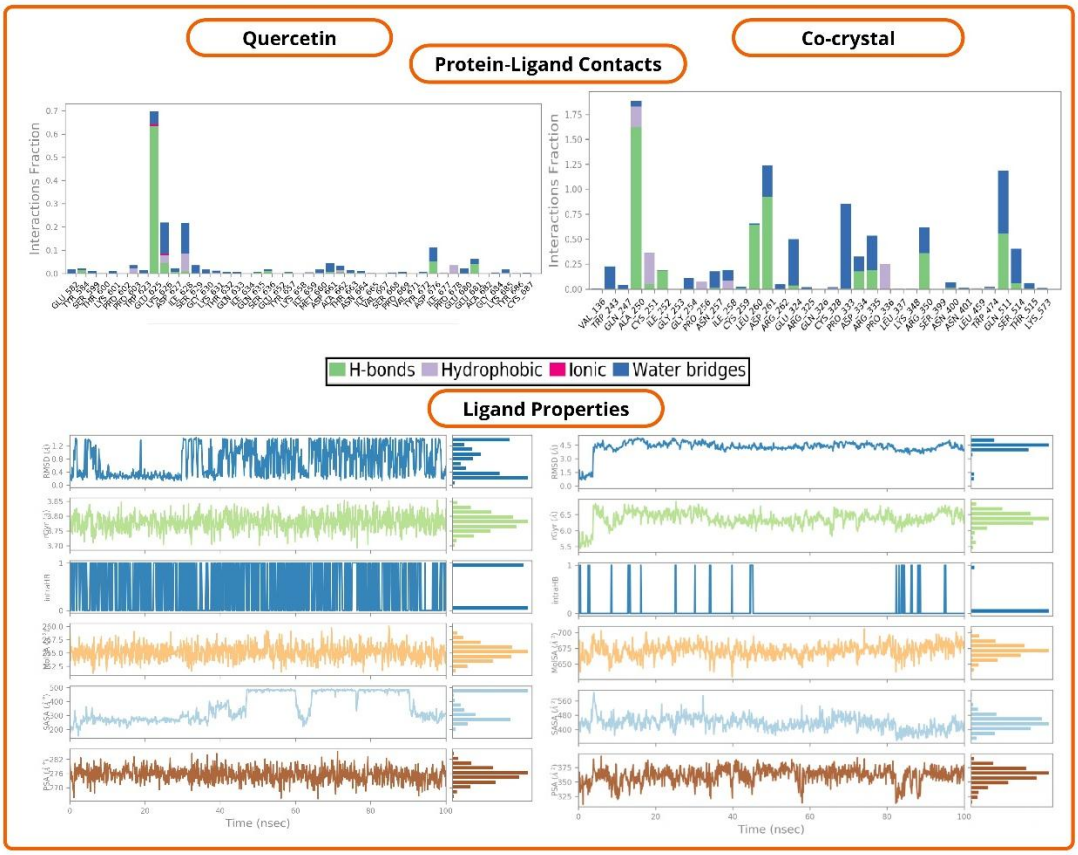

Figure 12: Protein–ligand interaction profile and ligand property analysis of quercetin and the co-crystal

3.5.4 MM-GBSA - Binding Free Energy Analysis

The Molecular Mechanics Generalized Born Surface Area (MM-GBSA) method was applied to calculate the binding free energies of quercetin and the co-crystallized ligand in complex with STAT3. This provides a quantitative assessment of binding affinity and energetic stability (**Table 7** and **Figure 13**).

The calculated total binding free energy (ΔG_bind) for the quercetin–STAT3 complex was −75.16 kcal/mol, which was slightly more than the co-crystal complex (−74.22 kcal/mol). The more negative binding free energy observed for quercetin indicates a strong and energetically stable interaction with the STAT3 binding site. Evaluation of the individual energy components showed that complex stabilization was mainly driven by van der Waals interactions. Quercetin exhibited a van der Waals energy contribution of −49.62 kcal/mol, which was comparable to that of the co-crystallized ligand (−50.06 kcal/mol). Lipophilic interactions were observed for quercetin (−30.07 kcal/mol) and the co-crystallized ligand (−29.85 kcal/mol), further supporting the importance of hydrophobic complementarity in ligand binding.

The Coulombic energy for the quercetin complex was −20.25 kcal/mol, slightly more favorable when compared with the co-crystallized complex (−19.85 kcal/mol), reflecting stronger electrostatic interactions among the STAT3 binding cavity. Hydrogen-bonding contributions were relatively modest, with values of −1.93 kcal/mol for quercetin and −2.02 kcal/mol for the co-crystal ligand. This suggest the hydrogen bonds also contribute to binding stability.

The covalent energy term showed values for quercetin (−5.06 kcal/mol) and the co-crystallized ligand (−4.92 kcal/mol), indicating comparable internal energetic contributions in both complexes. The MM-GBSA results demonstrate that quercetin forms a highly stable complex with STAT3, exhibiting a binding free energy slightly etter to that of the co-crystallized ligand.

Table 7: Average MM-GBSA Binding Free Energies of Quercetin and the Co-crystallized Ligand

Compound code	ΔGbind free energy (kcal/mol)	ΔGbind Coulomb (kcal/mol)	ΔGbind Covalent (kcal/mol)	ΔGbind VdW (kcal/mol)	ΔGbind H-bond (kcal/mol)	ΔGbind Lipophilic (kcal/mol)
Quercetin	-75.16	-20.25	-5.06	-49.62	-1.93	-30.07
Co-crystal	-74.22	-19.85	-4.92	-50.06	-2.02	-29.85

3.5.5 Principal Component Analysis (PCA)

Principal Component Analysis (PCA) was used to characterize the large-scale conformational motions and dynamic behaviour of the quercetin–STAT3 and co-crystal–STAT3 complexes throughout the simulation (**Figure 13**). PCA reduces the complexity of molecular motions into a few principal components (PCs), allowing visualization of dominant conformational transitions sampled during the simulation.

For the quercetin–STAT3 complex, the conformational ensemble remained relatively confined within the ranges of approximately −60 to +60 along PC1, −40 to +40 along PC2, and −30 to +20 along PC3. The trajectory initially occupied regions characterized by positive PC1 and PC2 values during the first 20 ns, indicating an early stable conformational state. As the simulation progressed, gradually shifted toward neutral PC2 values around 40 ns, followed by sampling in the negative PC1 and positive PC2 regions until the end of the simulation. The wider distribution suggests greater conformational variability compared with the quercetin complex; however, the presence of well-defined clusters was consistent with the preservation of structural integrity throughout the simulation.

The co-crystal–STAT3 complex, during the initial 20 ns, the conformations were primarily localized within the negative PC1 and PC3 regions while maintaining positive PC2 values. Around 40 ns, the system shifted toward regions with near-neutral PC1 values while continuing to sample positive PC2 and negative PC3 conformations. By approximately 70 ns, the trajectory migrated toward positive PC1 and PC2 regions. The overall conformational space sampled by the co-crystal complex was broader, extending from approximately −100 to +75 along PC1, −20 to +80 along PC2, and −60 to +20 along PC3. The wider distribution suggests greater conformational variability compared with the quercetin complex, although the presence of well-defined clusters indicates that the system remained structurally stable during the simulation period.

3.5.6 Free Energy Landscape (FEL) Analysis

The first two principal components (PC1 and PC2) were used as reaction coordinates to generate the Free Energy Landscape (FEL), enabling the evaluation of the conformational stability of the protein–ligand complexes over the simulation trajectory (**Figure 14**).The low-energy basins represent energetically favourable and stable conformations, whereas high-energy regions correspond to less favourable transitional states.

The FEL of the quercetin–STAT3 complex displayed a rugged landscape with conformational sampling distributed across PC1 values ranging from approximately −60 to +60 and PC2 values between −60 and +60. Several well-defined low-energy basins with the deepest minima occurring at approximately 2–4 kJ/mol, consistent with highly stable conformational states.Intermediate-energy regions ranging from 4 to 8 kJ/mol occupied a broader portion of the landscape, suggesting smooth transitions between energetically favourable conformations. Higher-energy conformations, between 10 and 12 kJ/mol, occupied a limited area, indicating less stable states.

The co-crystal–STAT3 complex also exhibited a rugged free energy landscape, with conformational sampling extending from approximately −100 to +50 along PC1 and from 0 to +80 along PC2. The lowest energy basins were observed around 20 kJ/mol, corresponding to stable conformational states sampled during the simulation. Intermediate-energy regions ranging from approximately 21.5 to 23 kJ/mol, indicating continuous transitions among closely related structural states. Higher-energy conformations, observed between 23 and 24 kJ/mol, appeared as localized peaks and represented less favourable structural arrangements.

The FEL analysis revealed that quercetin–STAT3 complex displayed multiple deep energy minima and a relatively confined conformational distribution, supporting its stable binding behaviour and favourable thermodynamic behaviour than cocrystal ligand.

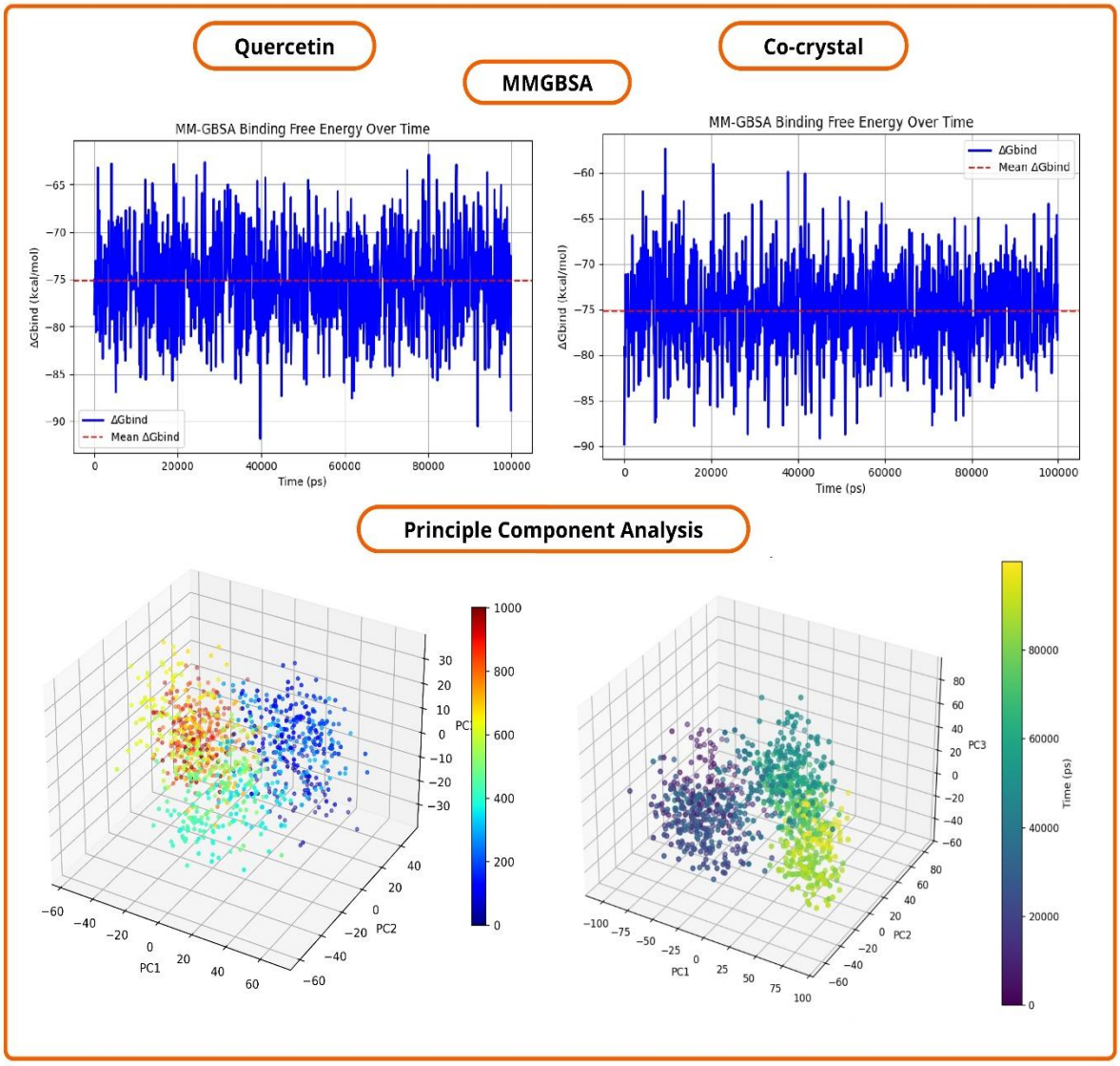

Figure 13: MM-GBSA and PCA analyses of quercetin and the co-crystallized ligand

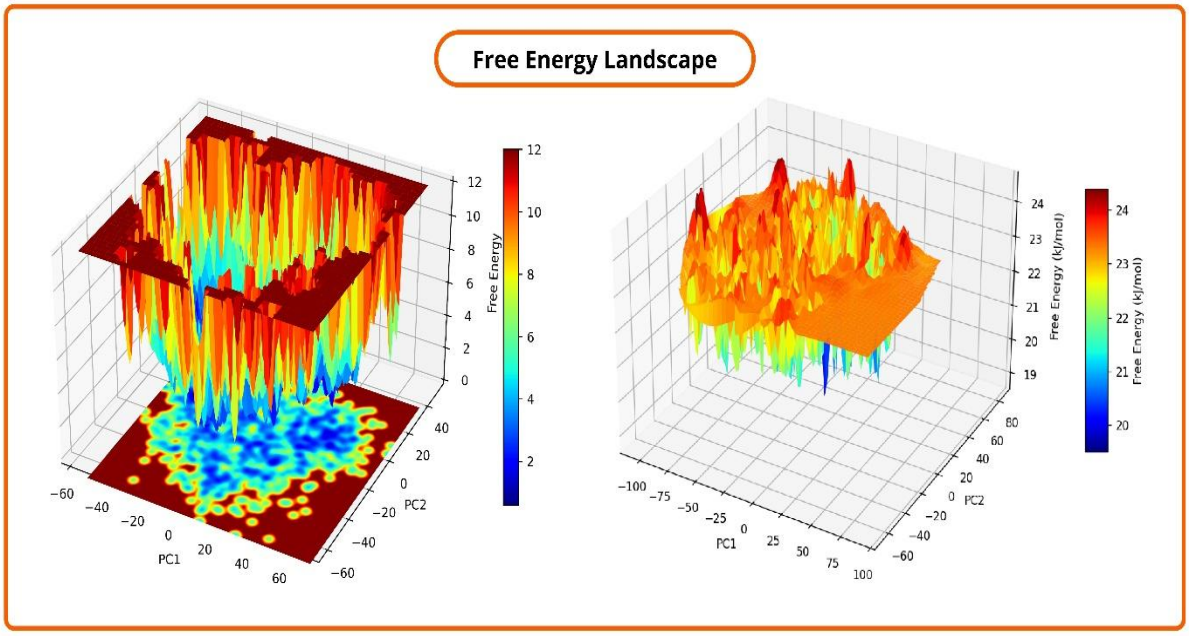

Figure 14: FEL plots for the quercetin and the cocrystal

3.5.7. ADMET Analysis

The ADMET profiles of the selected phytoconstituents and the standard drug, ethosuximide, were predicted using the pkCSM web server, and the findings are summarized in (**Table 8)**. The selected compounds exhibited diverse pharmacokinetic characteristics with varying absorption, distribution, metabolism, and toxicity profiles. Human intestinal absorption (HIA) ranged from 54.128 to 100.000, with betaine (100.000), elemicin (95.971), scopoletin (95.277), acetyl eugenol (94.755), and 4-hydroxycinnamic acid (93.494) demonstrating high predicted intestinal absorption, comparable to the standard drug, ethosuximide (93.148).

The predicted logBB values, representing blood brain barrier (BBB) permeability, varied from −1.377 to 0.407. Acetyl eugenol (0.401), thymol (0.407), and elemicin (0.368) exhibited relatively higher BBB permeability, suggesting a greater predicted ability to penetrate the central nervous system, whereas quercetin (−1.098) and gallocatechin (−1.377) showed comparatively lower BBB permeability, indicating limited predicted brain penetration. The predicted Caco-2 permeability values ranged from −0.375 to 1.859, with elemicin (1.859), acetyl eugenol (1.659), and thymol (1.606) exhibiting relatively higher permeability.None of the selected phytoconstituents or the

standard drug were predicted to inhibit CYP3A4. However, quercetin, scopoletin, acetyl eugenol, thymol, and elemicin were predicted to inhibit CYP1A2, whereas the remaining compounds were predicted to be non-inhibitors. Toxicity prediction indicated that most of the selected phytoconstituents were negative for AMES toxicity and hepatotoxicity. However, elemicin showed a positive AMES toxicity prediction, while thymol was predicted to be hepatotoxic. Overall, the ADMET analysis suggested that the majority of the selected phytoconstituents possess favorable pharmacokinetic characteristics with acceptable predicted safety profiles, supporting their further investigation as potential anticonvulsant candidates.

Table 8: ADMET Profiles of Selected Phytochemicals and Ethosuximide

Reference Drug / Selected Phytoconstituents	**BBB Permeability (logBB)**	**Caco-2 (logPapp)**	**HIA %**	**CYP3A4 Inhibitions**	**CYP1A2 Inhibitions**	**AMES Toxicity**	**Hepatotoxicity**
Ethosuximide**	-0.238	1.19	93.148	No	No	Negative	Negative
Quercetin	-1.098	-0.229	77.207	No	Yes	Negative	Negative
Scopoletin	-0.299	1.184	95.277	No	Yes	Negative	Negative
Gallocatechin	-1.377	-0.375	54.128	No	No	Negative	Negative
Acetyl eugenol	0.401	1.659	94.755	No	Yes	Negative	Negative
4hydroxycinnamic acid	-0.225	1.21	93.494	No	No	Negative	Negative
Thymol	0.407	1.606	90.843	No	Yes	Negative	Positive
Elemicin	0.368	1.859	95.971	No	Yes	Positive	Negative
Protocatechuic acid	-0.683	0.49	71.174	No	No	Negative	Negative
Caffeic acid	-0.647	0.634	69.407	No	No	Negative	Negative
Betaine	-0.214	1.44	100	No	No	Negative	Negative

Ethosuximide**: Reference Drug

4.1. Comparison of Seizure Latency and Seizure Duration in the PTZ-Induced Seizure Model

Table 9:

Experimental Groups	Seizure Onset (s)	Seizure Duration (s)
Vehicle Control Distilled water (10 mL/kg, p.o.)	48.167±5.043	302.83±66.847
Standard Ethosuximide (150mg/kg)	0.000***	0.000***
Low dose *Chenopodium album* L., 100mg/kg,p.o	95.000±6.875*	220.83±15.728*
Medium dose *Chenopodium album* L.,200mg/kg,p.o	112.00± 39.175**	146.50±48.952**
High dose *Chenopodium album* L., 400mg/kg,p.o	0.000***	0.000***
Data are presented as mean ± SEM (n = 6 mice per group). Statistical analysis was performed using one-way ANOVA followed by Tukey's multiple comparison test. NS=Non significant (P>0.05),*P<0.05, **P<0.01***P<0.001 vs. the control group.		

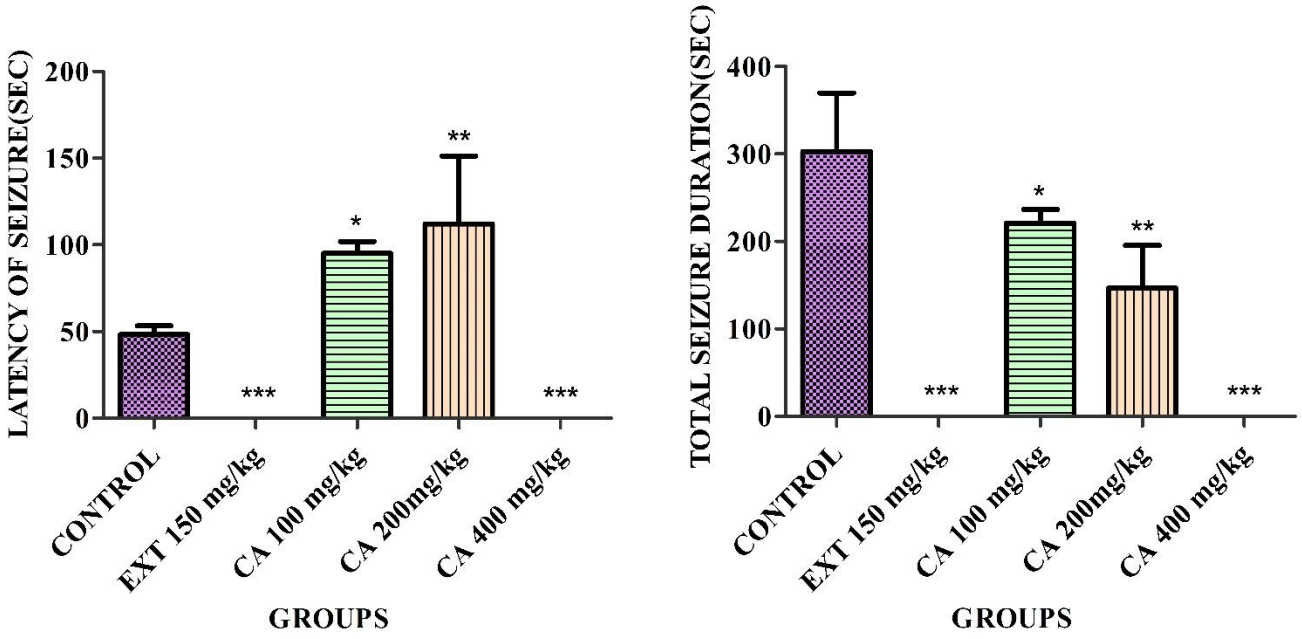

Figure 15. Effect of *Chenopodium album* L. on **seizure latency** (a) and **total seizure duration** (b) in the PTZ dose-optimization model. Bars represent mean ± SEM values (n = 6). Statistical significance was evaluated by one-way ANOVA followed by Tukey's multiple comparison test (compared with control group). NS = Non-significant ($p > 0.05$); *$p < 0.05$ (significant); **$p < 0.01$ (highly significant); ***$p < 0.001$ (very highly significant), 0 (no seizure).

In the PTZ-induced seizure model, mice administered distilled water served as the control group showed rapid seizure onset, with individual latencies ranging from 40–66 seconds (mean 48.17 ± 5.04 s). Seizure severity was high (grades 4–6), and seizure durations ranged from 249–448 seconds (mean 302.83 ± 66.85 s). One untreated control mouse developed a grade-6 seizure and died, confirming the strong convulsant action of PTZ, while no mortality occurred in the remaining control animals.

Ethosuximide (150 mg/kg) produced complete protection, as all six mice showed grade 0 severity, with no seizure latency or duration recorded (0.00 s), and no mortality, validating the responsiveness of the model.

Chenopodium album extract exhibited a clear dose-dependent anticonvulsant effect. Treatment with 100 mg/kg prolonged seizure latency to 95.00 ± 6.88 s. with severity grades ranging from 1–4, and the mean seizure duration reduced to 220.83 ± 15.73 s. All animals survived.

At the 200 mg/kg dose, seizure onset was further delayed, with a mean latency of 112.00 ± 39.18 s., severity decreased markedly (grades 0–1), and two out of six mice showed complete protection with no seizures. Among animals that seized, durations ranged from 169–280 seconds, giving a mean of 146.50 ± 48.95 s.

At the highest dose (400 mg/kg), *Chenopodium album* produced complete protection against seizures, as all animals were assigned a seizure score of grade 0, and no seizure onset or duration recorded (0.00 s), comparable to ethosuximide. No mortality occurred in any treated group. **(Supplementary table –T2)**

Overall, *Chenopodium album* extract markedly delayed the onset of seizures and significantly decreased seizure duration and severity, and provided full protection at 400 mg/kg, demonstrating progressively greater anticonvulsant activity across the tested doses in the PTZ model.

4.2. Effect of Combined Treatment with *Chenopodium album* and Ethosuximide on Seizure Latency and Duration in the PTZ Model

Table 10:

Experimental Groups	Seizure Onset (s)	Seizure Duration (s)
Vehicle Control, Distilled water (10 mL/kg, p.o.)	48.167±5.043	383.40±21.363
Standard (100%ETX),150mg/kg, p.o	0.000***	0.000***
CA 100% (400 mg/kg, p.o.)	0.000***	0.000***
50%CA+ 50% ETX (200 mg/kg, p.o. + 75 mg/kg, p.o.)	95.000±43.493**	86.667±55.056 ***
25% CA+75% ETX (100 mg/kg, p.o. + 112.5 mg/kg, p.o.)	92.500±41.566**	99.500±44.734***
75% CA+ 25% ETX (300 mg/kg, p.o. + 37.5 mg/kg, p.o.)	110.83±70.100***	56.667±56.667***
Data are presented as mean ± SEM (n = 6 mice per group). Statistical analysis was performed using one-way ANOVA followed by Tukey's multiple comparison test. NS=Non significant (P>0.05),*P<0.05, **P<0.01***P<0.001 vs. the control group.		

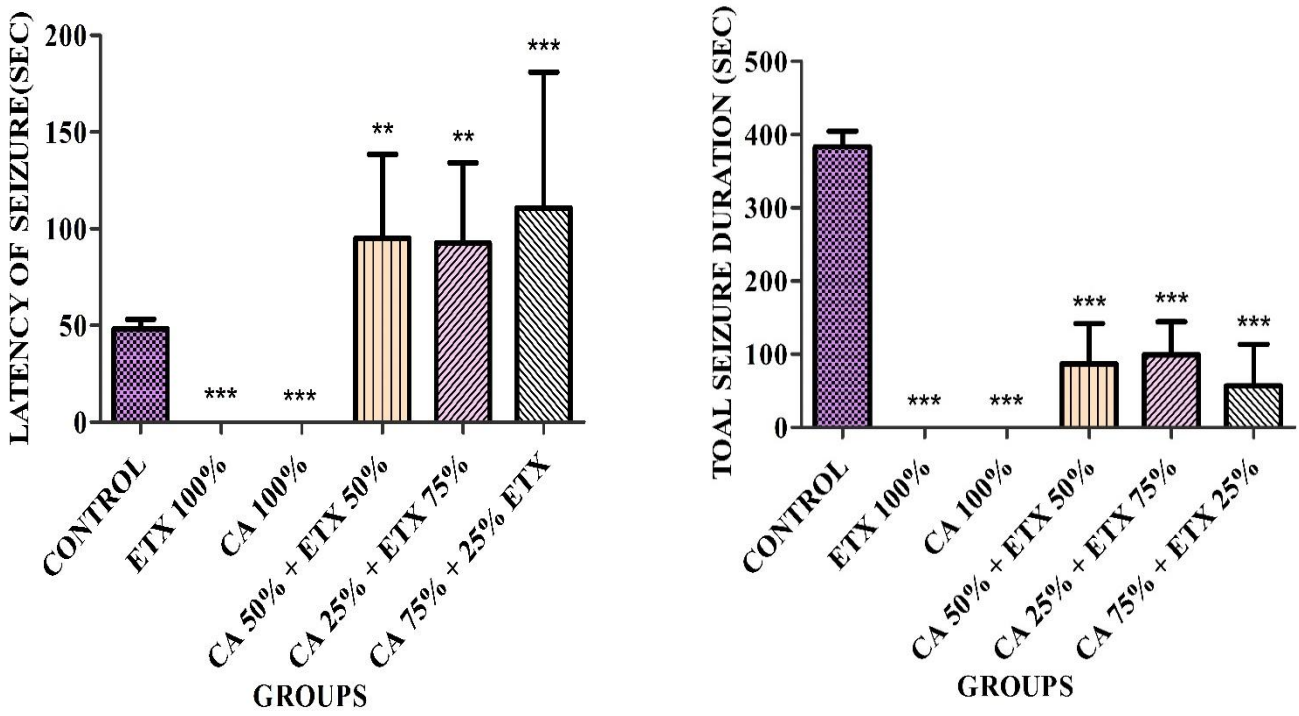

Figure 16. Effect of *Chenopodium album* L. on seizure latency (a) and total seizure duration (b) in the PTZ dose-optimization model. Bars represent mean ± SEM values (n = 6). Statistical significance was evaluated by one-way ANOVA followed by Tukey's multiple comparison test (compared with control group). NS = Non-significant ($p > 0.05$); *$p < 0.05$ (significant); **$p < 0.01$ (highly significant); ***$p < 0.001$ (very highly significant), 0 (no seizure).

In the PTZ model, the control group exhibited a mean latency to seizure onset of 48.16 ± 5.04 seconds and a mean seizure duration of 383.40 ± 21.36 seconds, confirming a strong susceptibility to chemically induced seizures. Both the Ethosuximide-treated group (150 mg/kg) and the 100% *Chenopodium album*-treated group (400 mg/kg) exhibited complete protection against PTZ-induced seizures, with no seizures observed. Compared with the control group, both treatments produced a highly significant anticonvulsant effect ($P < 0.001$).

Combination treatment groups also exhibited improved seizure resistance, though not complete protection. In the 50% CA: 50% ETX group, the mean seizure latency increased to 95.00 ± 43.49 seconds ($P<0.01$), while the duration was significantly reduced to 86.67 ± 55.05 seconds ($P<0.001$). Similarly, the 25% CA: 75% ETX group showed a latency of 92.50 ± 41.56 seconds ($P<0.01$) and duration of 99.50 ± 44.73 seconds ($P<0.001$). The 75% CA: 25% ETX group demonstrated the highest latency among the combination treatments (110.83 ± 70.10 seconds, $P<0.001$) and the lowest seizure duration (56.67 ± 56.67 seconds, $P<0.001$), indicating a strong anticonvulsant response.

Although the full-dose *Chenopodium album* extract provided complete protection, the combination groups did not achieve 100% seizure abolition. However, the seizures observed in these groups were very mild, falling within grade 0–2**,** indicating only minor motor responses rather than full convulsive episodes. This outcome may be attributed to the reduced extract dose in the combination treatments, resulting in an additive rather than complete protective effect when administered with ethosuximide. (**Supplementary table –T3**)

Overall, the findings confirm that *Chenopodium album* extract possesses significant anticonvulsant activity in the PTZ model, where the highest tested dose achieved complete seizure protection comparable to that of Ethosuximide. Combination treatment also demonstrated beneficial effects by delaying seizure onset and reducing severity and duration, supporting the potential application of *Chenopodium album* as an effective anticonvulsant candidate either independently or in adjunct therapy.

5. Discussion:

Chenopodium album L. was selected for this study based on its traditional use in folk medicine [2] and reported central nervous system–modulating activities such as sedative and antidepressant effects[11],suggesting the presence of neuroactive phytoconstituents relevant to seizure modulation. The identification of 26 phytoconstituents using LC-MS, along with their druggability prediction, marks a significant advancement in the investigation of this plant for anti-epileptic potential. The identified phytoconstituents fulfilled the criteria of Lipinski's Rule of Five, reflecting favorable pharmacokinetic behavior and supporting their potential as drug-like therapeutic agents [47].Notably, several phytoconstituents identified in the extract including alpha-pinene [48],caffeic acid [49],leucine [50],linalool [51],lupeol [52], oleanolic acid [53],quercetin[54], thymol [55], vanillin [56], and gallocatechin [57] have previously been reported to possess anticonvulsant, neuroprotective, or neuromodulatory activity. However, their collective presence in *Chenopodium album*, a plant not extensively investigated for epilepsy, provides novel evidence that it may act as a multitarget natural therapeutic development. The extract yield of 32.72% (w/w) reflects efficient recovery of bioactive constituents, consistent with earlier studies reporting methanol as a commonly used solvent for extracting diverse phytochemicals from *Chenopodium album* [58].

Network pharmacology has emerged as an effective systems biology strategy for investigating the multi-component and multi-target mechanisms of medicinal plants. In this study, 26

phytoconstituents identified from *C. album* generated 712 putative protein targets, of which 541 overlapped with epilepsy-associated genes. The substantial overlap between phytochemical-associated targets and epilepsy-related genes suggests that *C. album* may regulate multiple biological processes involved in epileptogenesis rather than acting through a single molecular target. The protein-protein interaction network further revealed extensive interactions among the common targets, indicating coordinated regulation of signalling pathways involved in neuronal survival, neuroinflammation, apoptosis, and synaptic plasticity.

Network topology analysis identified STAT3, EGFR, HSP90AA1, AKT1, CTNNB1, SRC, IL6, ESR1, EP300, and BCL2 as the principal hub genes, with STAT3 exhibiting the highest degree score. Persistent activation of the JAK/STAT3 signalling pathway has been associated with seizure-induced neuroinflammation, astrocyte activation, blood-brain barrier dysfunction, and neuronal hyperexcitability. Similarly, IL6 is a major pro-inflammatory cytokine implicated in seizure progression, whereas EGFR, AKT1, and SRC regulate neuronal survival, proliferation, and intracellular signalling pathways involved in epileptogenesis. HSP90AA1, CTNNB1, ESR1, EP300, and BCL2 contribute to neuronal protection through regulation of apoptosis, transcriptional activity, protein stability, and neuroplasticity. These observations suggest that modulation of these interconnected signalling molecules may contribute to the anticonvulsant activity of *C. album*.

Gene Ontology (GO) analysis demonstrated significant enrichment in biological processes related to the overlapping targets in biological processes associated with negative regulation of apoptosis, transcriptional regulation, and positive regulation of gene expression, cell proliferation, and intracellular signalling. Analysis of the Cellular Component category indicated that the the common targets were primarily localized to the cytosol, nucleus, plasma membrane, and protein-containing complexes. In the Molecular Function category, the identified targets were mainly associated with protein binding, transcription factor binding, enzyme binding, ATP binding, and ubiquitin protein ligase binding. These findings indicate that the identified targets participate in extensive signalling networks responsible for maintaining neuronal function and cellular homeostasis.

Analysis of KEGG pathways identified that the overlapping targets were significantly enriched in pathways associated with epilepsy pathogenesis. Among these, EGFR tyrosine kinase inhibitor resistance showed the highest enrichment score, indicating the importance of EGFR-mediated

signalling in regulating neuronal survival and inflammatory responses. Other significantly enriched pathways included the JAK-STAT signalling pathway, HIF-1 signalling pathway, and estrogen signalling pathway, which collectively regulate neuroinflammation, oxidative stress, synaptic plasticity, and neuronal protection. These findings suggest that the therapeutic effects of *C. album* are mediated through the coordinated regulation of multiple signalling pathways rather than by targeting a single molecular pathway.

Molecular docking analysis demonstrated that quercetin exhibited the strongest binding affinity toward STAT3 among the 26 phytoconstituents evaluated. The formation of hydrogen bonds and water-mediated interactions with key residues, including Glu625, Lys626, and Ile628, contributed to favourable stabilization of the ligand within the STAT3 binding pocket. Although the co-crystallized ligand established a greater number of hydrogen-bond interactions, quercetin exhibited a comparable binding orientation and stable interaction profile, suggesting its potential to modulate STAT3 activity effectively.

The molecular docking findings were subsequently assessed using a 100 ns molecular dynamics simulation. RMSD analysis demonstrated that both the quercetin–STAT3 complex and the co-crystallized ligand complex remained structurally stable throughout the simulation. RMSF analysis indicated limited residue fluctuations, suggesting preservation of the overall protein architecture. Persistent hydrogen bonding together with hydrophobic, ionic, and water-mediated interactions involving key amino acid residues contributed to the stability of the quercetin-bound complex. Ligand property analysis further revealed that quercetin maintained a compact molecular conformation with minimal structural fluctuations, indicating stable accommodation within the STAT3 binding pocket.

MM-GBSA calculations provided additional evidence supporting the stability of the quercetin–STAT3 complex. The calculated binding free energy of −75.16 kcal/mol was slightly more favourable than that of the co-crystallized ligand (−74.22 kcal/mol), indicating spontaneous and energetically stable binding. Van der Waals interactions represented the major energetic contribution, while lipophilic and Coulombic interactions further enhanced ligand stabilization. Although hydrogen-bond contributions were comparatively smaller, they played an important role in maintaining specific ligand–protein interactions during the simulation period. Collectively, the obtained results demonstrate that quercetin maintains a stable interaction with STAT3 and is likely to contribute to the biological effects of *C. album*.

Principal component analysis demonstrated that the quercetin–STAT3 complex occupied a relatively confined conformational space compared with the co-crystallized ligand, indicating controlled conformational flexibility while maintaining structural stability throughout the simulation. Similarly, free energy landscape analysis revealed multiple deep low-energy basins and a comparatively restricted energy landscape for the quercetin complex, reflecting enhanced thermodynamic stability and favourable conformational transitions. These observations further support the stable interaction between quercetin and STAT3 predicted by molecular docking and molecular dynamics simulation.

The ADMET analysis demonstrated favourable pharmacokinetic characteristics for the majority of the selected phytoconstituents. Most compounds exhibited high predicted human intestinal absorption together with acceptable Caco-2 permeability, suggesting favourable oral bioavailability. Although BBB permeability varied among the compounds, acetyl eugenol, thymol, and elemicin demonstrated comparatively higher predicted penetration into the central nervous system, which is advantageous for the treatment of neurological disorders. None of the evaluated compounds inhibited CYP3A4, indicating a relatively low potential for CYP3A4-mediated drug interactions. Most phytoconstituents were identified as to be non-mutagenic and non-hepatotoxic, although elemicin exhibited positive AMES toxicity and thymol showed predicted hepatotoxicity, indicating that further experimental toxicological evaluation is warranted. Overall, the ADMET findings support the drug-like properties and pharmacokinetic suitability of the majority of the bioactive constituents identified in *C. album*.

The computational findings were strongly supported by the *in vivo* pharmacological evaluation in the PTZ-induced seizure model. PTZ produced rapid seizure onset, prolonged seizure duration, severe seizure scores, and mortality in untreated animals, confirming successful induction of seizures. In contrast, *C. album* extract produced a clear dose-dependent anticonvulsant effect characterized by delayed seizure onset, reduced seizure duration, decreased seizure severity, and complete prevention of mortality. The highest dose (400 mg/kg) completely abolished PTZ-induced seizures and provided protection comparable to ethosuximide. Furthermore, combination treatment with *C. album* extract and ethosuximide significantly improved seizure resistance by prolonging seizure latency and reducing seizure duration and severity, although complete protection was not achieved at the reduced extract doses. These findings indicate that *C. album*

possesses potent anticonvulsant activity and may serve as a useful adjunct to conventional antiepileptic therapy.

Overall, the integration of network pharmacology, molecular docking, molecular dynamics simulation, MM-GBSA, PCA, FEL, ADMET prediction, and *in vivo* pharmacological evaluation provides comprehensive evidence supporting the anticonvulsant potential of *Chenopodium album*. The findings suggest that the anticonvulsant activity of *C. album* is mediated through the synergistic action of multiple phytoconstituents that regulate neuroinflammation, neuronal survival, apoptosis, and intracellular signalling pathways, particularly through modulation of STAT3-associated signalling. These results indicate a strong scientific basis for the traditional use of *C. album* and support its further investigation as a promising multi-target therapeutic candidate for epilepsy.

6. Conclusion: The present study demonstrated that *Chenopodium album* possesses significant anticonvulsant potential through an integrated computational and experimental approach. Network pharmacology identified STAT3 as a key therapeutic target, while molecular docking, molecular dynamics simulation, MM-GBSA, PCA, and FEL analyses confirmed the stable interaction of quercetin with STAT3. ADMET prediction indicated favorable pharmacokinetic properties for most of the selected phytoconstituents. Furthermore, the methanolic extract exhibited significant dose dependent anticonvulsant activity in the PTZ induced seizure model, with complete seizure protection observed at 400 mg/kg, comparable to that of ethosuximide. Collectively, these findings suggest that *Chenopodium album* is a promising source of multi-target anticonvulsant agents and warrants further investigation to isolate its active constituents and validate their therapeutic potential in advanced preclinical and clinical studies.

List of abbreviations:

ADMET	Absorption, distribution, metabolism, excretion, and toxicity
AMES toxicity	Ames test for mutagenicity
ANOVA	Analysis of variance
CA/*C.album*	*Chenopodium album*
Caco-2	Human Colorectal Adenocarcinoma Cell Line-2
CPCSEA	Committee for the Purpose of Control and Supervision of Experiments on Animals

ETX	Ethosuximide
IAEC	Institutional Animal Ethics Committee
IMPATT	Indian Medicinal Plants, Phytochemistry and Therapeutics
KEGG	Kyoto Encyclopedia of Genes and Genomes
LC–MS	Liquid Chromatography–Mass Spectrometry
MM-GBSA	Molecular Mechanics/Generalized Born Surface Area
MW	Molecular weight
p.o.	Per oral
PTZ	Pentylenetetrazole
SEM	Standard Error of Mean
SMILES	Simplified Molecular Input Line Entry System
STAT3	Signal Transducer and Activator of Transcription 3

Acknowledgement

The authors sincerely acknowledge Visveswarapura Institute of Pharmaceutical Sciences, Bengaluru, for providing the necessary facilities and support to carry out this research work.

Authors contributions:

Naznin Sarkar: Writing-original draft, Software, Methodology, Formal analysis, Data curation. **Anil Kumar Venkategowda Kodihally**: Writing-review & editing, Methodology, Data curation, Conceptualization. **Bharath Kumar Chagaleti**: Writing-original draft, Methodology, Formal analysis, Data curation.

Funding

No external funding was received for this research. The study was carried out without financial assistance from governmental, commercial, or not-for-profit organizations.

Data availability

The data underlying this study are presented within the article and accompanying supplementary materials. Additional datasets are available from the corresponding author on reasonable request.

AI tool disclosure

AI-assisted tools were used only to enhance linguistic quality and clarity of the manuscript. They had no role in the study design, data analysis, interpretation, or in drawing the conclusions of this research.

Declaration of competing interest

The authors declare no competing interests related to this study. No external financial support was received from any public, commercial, or non-profit funding agencies. All animal experiments were performed in compliance with institutional ethical standards, with prior approval from the Institutional Animal Ethics Committee (IAEC).

Ethical approval

All experimental procedures were approved by the Institutional Animal Ethics Committee (IAEC) of Visveswarapura Institute of Pharmaceutical Sciences (VIPS), registered with CCSEA (Registration No. 152/PO/ReBi/S/99/CCSEA; originally dated 22/07/1999 and renewed on 22/12/2023). The study received ethical clearance under Project Proposal No. VIPS/IAEC/27–04–2024/25-AKV and Ref. No. VIPS/71/2024–25.

Supplementary materials

The Supporting Information is available as supplementary documents. It includes Drug-Likeness Analysis of Selected Phytoconstituents (**Table T1**) and Statistical Data (**Tables T2 and T3**).

References

1. Xie S, Zhan F, Zhu J, Xu S, Xu J (2025) The latest advances with natural products in drug discovery and opportunities for the future: a 2025 update. Expert Opin Drug Discov 20:827–843. https://doi.org/10.1080/17460441.2025.2507382
2. Chihomvu P, Ganesan A, Gibbons S, Johansson MJ, Woollard K, Hayes MA (2024) Phytochemicals in drug discovery: a confluence of traditional knowledge and modern methodologies. Int J Mol Sci 25:8792. https://doi.org/10.3390/ijms25168792
3. Poonia A, Upadhayay A (2015) *Chenopodium album* Linn: review of nutritive value and biological properties. J Food Sci Technol 52:3977–3985. https://doi.org/10.1007/s13197-014-1553-x
4. Kaur S, Shri R (2015) *Chenopodium album* L.: a review of pharmacological properties. Int J Pharm Sci Rev Res 33:49–54.
5. Aman F, Ullah N, Ahmad M, *et al* (2016) Ethnopharmacological profile of *Chenopodium album*: a comprehensive review. J Ethnopharmacol 193:713–725.
6. Akbaş P, Kaya E, Makav M, Yıldız G (2023) Investigation of antimicrobial and antioxidant activities of *Chenopodium album* extracts and their effects on gentamicin nephrotoxicity in rats. Food Sci Nutr 11:8121–8130. **https://doi.org/10.1002/fsn3.3733**

7. Kim SA, Choi SC, Youn YH, et al (2017) Antioxidant and anti-inflammatory effects of *Dioscorea japonica* and *Chenopodium album*. J Soc Cosmet Sci Korea 43:337–347.
8. Dash UC, Bhol NK, Swain SK, Samal RR, Nayak PK, Raina V, et al (2025) Oxidative stress and inflammation in the pathogenesis of neurological disorders: mechanisms and implications. Acta Pharm Sin B 15:15–34. https://doi.org/10.1016/j.apsb.2024.10.004
9. Ji D, Mylvaganam S, Ravi Chander P, Tarnopolsky M, Murphy K, Carlen P (2025) Mitochondria and oxidative stress in epilepsy: advances in antioxidant therapy. Front Pharmacol 15:1505867. https://doi.org/10.3389/fphar.2024.1505867
10. Li W, Wu J, Zeng Y, Zheng W (2023) Neuroinflammation in epileptogenesis: from pathophysiology to therapeutic strategies. Front Immunol 14:1269241. https://doi.org/10.3389/fimmu.2023.1269241
11. Sharma A, Kaur S, Shri R (2021) Evaluation of antidepressant activity of *Chenopodium album* extracts and fractions in mice. Int J Pharm Sci Res 12:2707–2715. https://doi.org/10.13040/IJPSR.0975-8232.12(5).2707-15
12. Ahmad M, Mohiuddin OA, Mehjabeen, Jahan N, Anwar M, Habib S, Alam SM, Baig IA (2012) Evaluation of spasmolytic and analgesic activity of ethanolic extract of *Chenopodium album* Linn. and its fractions. J Med Plants Res 6:4691–4697. https://doi.org/10.5897/JMPR12.412
13. Baldi A, Choudhary NK (2013) *In vitro* antioxidant and hepatoprotective potential of *Chenopodium album* extract. Int J Green Pharm 7:50–56. https://doi.org/10.4103/0973-8258.111614
14. Shi YQ, Yang HC, He C, Wang YH, Zheng J, Wang XY, *et al* (2025) Inflammatory links between epilepsy and depression: a review of mechanisms and therapeutic strategies. Front Neurosci 19:1614297. https://doi.org/10.3389/fnins.2025.1614297
15. Alkhaldi NA (2025) Navigating the depths: a comprehensive narrative review on depression in people with epilepsy. Heliyon 11:e41389. https://doi.org/10.1016/j.heliyon.2024.e41389
16. Sarkar N, Kodihally AK, Shamnewadi A (2025) Exploring the anticonvulsant potential of *Daucus carota* L.: a combined *in silico* and *in vivo* study for epilepsy therapy development. Pharmacol Res Mod Chin Med 15:100610. https://doi.org/10.1016/j.prmcm.2025.100610
17. De Bellis M, d'Orsi G, Rubino EM, Arigliano C, Carella M, Sciruicchio V, *et al* (2025) Adverse effects of antiseizure medications: a review of the impact of pharmacogenomics, drug–drug interactions, and clinical outcomes. Front Pharmacol 16:1589318. https://doi.org/10.3389/fphar.2025.1589318

18. Löscher W (2017) Animal models of seizures and epilepsy: past, present, and future role for the discovery of antiseizure drugs. Neurochem Res 42:1873–1888. https://doi.org/10.1007/s11064-017-2222-z
19. Van Erum J, Van Dam D, De Deyn PP (2019) PTZ-induced seizures in mice require a revised Racine scale. Epilepsy Behav 95:51–55. https://doi.org/10.1016/j.yebeh.2019.02.029
20. Velíšková J, Velíšek L (2017) Behavioral characterization and scoring of seizures in rodents. In: Pitkänen A, Buckmaster PS, Galanopoulou AS, Moshé SL (eds) Models of Seizures and Epilepsy**,** 2nd edn. Academic Press, Cambridge, pp 111–123.
21. Coulter DA, Huguenard JR, Prince DA (1989) Characterization of ethosuximide reduction of low-threshold calcium currents in thalamic neurons. Epilepsia 30:563–572. https://doi.org/10.1111/j.1528-1157.1989.tb05319.x
22. Mohanraj K, Karthikeyan BS, Vivek-Ananth RP, Bharath Chand RP, Aparna SR, Mangalapandi P, Samal A (2018) IMPPAT: a curated database of Indian medicinal plants, phytochemistry and therapeutics. Sci Rep 8:4329. https://doi.org/10.1038/s41598-018-22631-z
23. Kanagali SN, Patil BM, Khanal P, Unger BS (2022) *Cyperus rotundus* L. reverses the olanzapine-induced weight gain and metabolic changes: outcomes from network and experimental pharmacology. Comput Biol Med 141:105035. https://doi.org/10.1016/j.compbiomed.2021.105035
24. Daina A, Michielin O, Zoete V (2019) SwissTargetPrediction: updated data and new features for efficient prediction of protein targets of small molecules. Nucleic Acids Res 47:W357–W364. https://doi.org/10.1093/nar/gkz382
25. Gfeller D, Grosdidier A, Wirth M, Daina A, Michielin O, Zoete V (2014) SwissTargetPrediction: a web server for target prediction of bioactive small molecules. Nucleic Acids Res 42:W32–W38. https://doi.org/10.1093/nar/gku293
26. Rappaport N, Twik M, Plaschkes I, Nudel R, Iny Stein T, Levitt J, *et al* (2017) MalaCards: an amalgamated human disease compendium with diverse clinical and genetic annotation and structured search. Nucleic Acids Res 45:D877–D887. https://doi.org/10.1093/nar/gkw1012
27. Heberle H, Meirelles GV, da Silva FR, Telles GP, Minghim R (2015) InteractiVenn: a web-based tool for the analysis of sets through Venn diagrams. BMC Bioinformatics 16:169. https://doi.org/10.1186/s12859-015-0611-3

28. Dennis G Jr, Sherman BT, Hosack DA, Yang J, Gao W, Lane HC, *et al* (2003) DAVID: Database for Annotation, Visualization, and Integrated Discovery. Genome Biol 4:R60. https://doi.org/10.1186/gb-2003-4-9-r60
29. Szklarczyk D, Gable AL, Nastou KC, Lyon D, Kirsch R, Pyysalo S, *et al* (2021) The STRING database in 2021: customizable protein–protein networks, and functional characterization of user-uploaded gene/measurement sets. Nucleic Acids Res 49:D605–D612. https://doi.org/10.1093/nar/gkaa1074
30. Franz M, Lopes CT, Fong D, Kucera M, Cheung M, Siper MC, *et al* (2023) Cytoscape.js 2023 update: a graph theory library for visualization and analysis. Bioinformatics 39:btad031. https://doi.org/10.1093/bioinformatics/btad031
31. Laamari Y, Bimoussa A, Mourad F, Chagaleti BK, Saravanan V, Alossaimi MA, *et al* (2024) Multitargeted molecular docking and dynamics simulation of thymol-based chalcones against cancer protein markers: synthesis, characterization, and computational study. J Mol Struct 1317:139116. https://doi.org/10.1016/j.molstruc.2024.139116
32. Mukhrish YE, Al-Humaidi JY, Chagaleti BK, Albedair LA, Gomha SM, Saravanan V, *et al* (2025) Exploring the cyclization of thiosemicarbazone to 1,3,4-thiadiazole: synthesis, characterization and *in silico* study. J Mol Struct 1322:140385. https://doi.org/10.1016/j.molstruc.2024.140385.
33. Irrou E, Ait Elmachkouri Y, Blacque O, Kumer A, Chagaleti BK, MK K, *et al* (2025) Functionalized aromatic sulfones from 1,4-benzothiazine-3-one-1,1-dioxide: design, synthesis, crystal structure, and *in silico* evaluation against SARS-CoV-2 proteins. **ChemistrySelect** 10:e202503748. https://doi.org/10.1002/slct.202503748
34. Bellapukonda SM, Singothu S, Singampalli A, Bandela R, Kumar P, Yaddanapudi VM, *et al* (2025) Exploring spirocyclic isoquinoline-piperidine compounds in tuberculosis therapy: ADMET profiling, docking, DFT, MD simulations, and MMGBSA analysis. Comput Biol Chem 118:108447. https://doi.org/10.1016/j.compbiolchem.2025.108447.
35. Irrou E, Elmachkouri YA, Haddad SE, Chagaleti BK, Mague JT, MK K, *et al* (2025) Synthesis of novel N4-substituted and C2-disubstituted 1,4-benzothiazine-1,1-dioxide derivatives: integrative computational strategies for breast cancer therapy. J Mol Struct 1338:142310. https://doi.org/10.1016/j.molstruc.2025.142310
36. Sadula A, Chagaleti BK, Enneiymy M, Peddaboina UR, Ankireddy A, Al Ajmi MF, *et al* (2025) Multifaceted analysis of novel trisubstituted imidazole chromen derivatives: design, synthesis,

characterization, molecular docking, and antimicrobial evaluation. J Mol Struct 1346:143185. https://doi.org/10.1016/j.molstruc.2025.143185

37. Genheden S, Ryde U (2015) The MM/PBSA and MM/GBSA methods to estimate ligand-binding affinities. Expert Opin Drug Discov 10:449–461. https://doi.org/10.1517/17460441.2015.1032936
38. Bellapukonda SM, Singothu S, Singampalli A, Bandela R, Kumar P, Yaddanapudi VM, *et al* (2025) Exploring spirocyclic isoquinoline-piperidine compounds in tuberculosis therapy: ADMET profiling, docking, DFT, MD simulations, and MMGBSA analysis. Comput Biol Chem 118:108447. https://doi.org/10.1016/j.compbiolchem.2025.108447
39. Altharawi A, Chagaleti BK, Alamri MA, Riadi Y, Aldakhil T, Moulay Youssef AI, *et al* (2026) Synthesis, molecular modelling, and evaluation of new mono- and bis-isoxazolines as antibacterial agents: *in vitro* and *in silico* analysis. RSC Adv 16:26399–26420. https://doi.org/10.1039/D5RA09902A
40. Riadi Y, Rajesh R, Chagaleti BK, Altharawi A, Joseph D, Geesi MH, *et al* (2026) Exploration of a novel thiadiazole derivative: design, synthesis, biological evaluation (*in vitro* and *in silico*), and DFT studies. J Fluoresc 36:2605–2631. https://doi.org/10.1007/s10895-026-04708-5
41. Pires DEV, Blundell TL, Ascher DB (2015) pkCSM: predicting small-molecule pharmacokinetic and toxicity properties using graph-based signatures. J Med Chem 58:4066–4072. https://doi.org/10.1021/acs.jmedchem.5b00104
42. Rana S, Rahman S, Sana S, et al (2020) Anticancer potential of *Chenopodium album* leaf extract against Ehrlich ascites carcinoma cells in Swiss albino mice. Future J Pharm Sci 6:1–9. https://doi.org/10.1186/s43094-020-00079-8
43. Magama S, Asita AO (2017) Evaluation of *Chenopodium album* Linn. crude methanolic leaf extract for central antinociceptive activity in albino mice using the hot plate test. Int J Sci 6:36–44.
44. Shimada T, Yamagata K (2018) Pentylenetetrazole-kindling mouse model. In: Methods Mol Biol 1727:495–503. https://doi.org/10.1007/978-1-4939-7571-6_37
45. Mandhane SN, Aavula K, Rajamannar T (2007) Timed pentylenetetrazol infusion test: a comparative analysis with s.c. PTZ and MES models of anticonvulsant screening in mice. Seizure 16:636–644. https://doi.org/10.1016/j.seizure.2007.05.009
46. Sarkar N, Kodihally AK, Khan M (2025) Integrative evaluation of *Daucus carota* L. as an antiepileptic agent: *in silico* (network pharmacology, ADMET, molecular docking, MD simulation)

and *in vivo* correlation using PTZ-induced seizure model. In Silico Res Biomed 100140. https://doi.org/10.1016/j.insilr.2025.100140

47. Lipinski CA, Lombardo F, Dominy BW, *et al* (2001) Experimental and computational approaches to estimate solubility and permeability in drug discovery and development settings. Adv Drug Deliv Rev 46:3–26. https://doi.org/10.1016/S0169-409X(00)00129-0
48. Zamyad M, Abbasnejad M, Esmaeili-Mahani S, *et al* (2019) The anticonvulsant effects of *Ducrosia anethifolia* (Boiss.) essential oil are produced by its main component α-pinene in rats. Arq Neuropsiquiatr 77:106–114. https://doi.org/10.1590/0004-282X20190004
49. Coelho VR, Vieira CG, de Souza LP, *et al* (2015) Antiepileptogenic, antioxidant and genotoxic evaluation of rosmarinic acid and its metabolite caffeic acid in mice. Life Sci 122:65–71. https://doi.org/10.1016/j.lfs.2014.12.010
50. Hartman AL, Santos P, O'Riordan KJ, *et al* (2015) Potent anti-seizure effects of D-leucine. Neurobiol Dis 82:46–53. https://doi.org/10.1016/j.nbd.2015.05.013
51. Elisabetsky E, Brum LF, Souza DO (1999) Anticonvulsant properties of linalool in glutamate-related seizure models. Phytomedicine 6:107–113. https://doi.org/10.1016/S0944-7113(99)80044-0
52. Elusiyan CA, Faria AL, Mendes AE, *et al* (2020) Involvement of the benzodiazepine site in the anticonvulsant activity of *Tapinanthus globiferus* against pentylenetetrazole-induced seizures in mice. Planta Med 86:1204–1215. https://doi.org/10.1055/a-1235-1942
53. Akünal Türel C, Yunusoğlu O (2023) Oleanolic acid suppresses pentylenetetrazole-induced seizure *in vivo*. Int J Environ Health Res 33:529–540. https://doi.org/10.1080/09603123.2021.2012434
54. Nieoczym D, Socała K, Raszewski G, *et al* (2014) Effect of quercetin and rutin in some acute seizure models in mice. Prog Neuropsychopharmacol Biol Psychiatry 54:50–58. https://doi.org/10.1016/j.pnpbp.2014.04.019
55. Sancheti J, Shaikh MF, Chaudhari R, *et al* (2014) Characterization of anticonvulsant and antiepileptogenic potential of thymol in various experimental models. Naunyn Schmiedebergs Arch Pharmacol 387:59–66. https://doi.org/10.1007/s00210-013-0928-5
56. Luszczki JJ, Wlodarczyk M, Glensk M, *et al* (2013) Effects of alizarin, betulin, curcumin, diosmin, linalool, menthofuran, α-terpineol, theobromine, β-thujaplicin and vanillin against maximal electroshock-induced seizures in mice. J Pre Clin Clin Res 7:27–31.

57. Taslimi P, Kocyigit UM, Tüzün B, *et al* (2022) Biological effects and molecular docking studies of catechin-5-*O*-gallate: antioxidant, anticholinergic, antiepileptic and antidiabetic potentials. J Biomol Struct Dyn 40:2489–2497. https://doi.org/10.1080/07391102.2020.1848184
58. Arora SK, Itankar PR, Yende SR. Phytochemical screening and TLC studies of different extracts of *Chenopodium album*. J Ayurvedic Herb Med. 2020; 6(1):15-20.

Supplementary Files

This is a list of supplementary files associated with this preprint. Click to download.

- SupplementarytableT1.docx
- SupplementaryTableT2.docx
- SupplementarytableT3.docx